



# Crashworthiness characteristics of composite cylindrical energy absorbers filled with honeycomb and foam under quasi-static load: experimental and analytical study

Reza Sarkhosh<sup>1</sup> · Amin Farrokhbadi<sup>1</sup> · Hamidreza Zarei<sup>2</sup>

Received: 15 March 2022 / Accepted: 27 June 2022 / Published online: 15 July 2022

This is a U.S. Government work and not under copyright protection in the US; foreign copyright protection may apply 2022

## Abstract

In this study, the crashworthiness characteristics of four cases including cylindrical hollow composite tubes, aluminum honeycomb-filled tubes, polyurethane foam-filled tubes, and polyurethane foam/aluminum honeycomb-filled cylindrical composite are experimentally investigated. The impact of honeycomb, polyurethane foam, combined polyurethane foam with honeycomb filling, and diameter and thickness of wall of cylindrical composites are also investigated. Then, the deformation mode, peak crushing force, mean crushing force (MCF), energy absorption (EA), and specific energy absorption of these composites possessing different structures are also explored. Furthermore, an analytical model for the crushing behavior of the cylindrical composite shell filled with foam and honeycomb materials under quasi-static load is provided. The analytical model which draws on the energy method is used to predict the MCF and crushing length during the collapse process. For this purpose, the diverse phenomena including shell bending, petal formation, circumferential delamination, friction, collapse of honeycomb cell walls, and deformation of foam are considered to determine the total internal energy relations during the crash process. These relations are used to make predictions on mean loads and total displacements during the collapse. The obtained results reveal a relatively good agreement between the analytical and experimental findings. The results showed that all novel cylindrical composite tubes filled with both polyurethane foam and aluminum honeycomb, in addition to increasing energy absorption compared to their counterparts, deform only in the stable mode of collapse (Mode I), which is a very important predictable deformation in terms of design.

**Keywords** Mean crushing force · Quasi-static load · Cylindrical composite · Foam · Honeycomb · Energy absorption

## 1 Introduction

In the early 1970s, awareness of energy absorbing in thin-walled tubes for crashworthiness applications grew due to increase in the safety in major transportation industries, such as automobiles, airlines, and aerospace [1]. Thin-walled structures are frequently applied for energy absorption (EA). Recently, there has been an increasing interest in the use of thin metal structures filled with foam to yield a viable

energy absorber with a roughly lower peak load. The average crushing stress and the half-wavelength of the metal hexagonal honeycomb folding mode subjected to out-of-plane quasi-static loading have been identified by Wierzbicki [2]. Wierzbicki suggested an analytical model that serves as the basis for all theoretical models for the study of these kinds of energy absorbers. Chen and Wierzbicki [3] argued that, while analyzing thin-walled structures, the determination of the flow stress yields more satisfactory description of the material behavior. Li et al. [4] performed a study on the dynamic crushing characteristics of honeycomb structures whose cells possessed irregular shapes non-uniform walls. Zarei Mahmoudabadi and Sadighi [5] explored metal hexagonal honeycomb crushing exposed to quasi-static loading. In this study, they analyzed two important parameters, i.e., the average crushing stress and the wavelength of the folding mode. Alavi Nia et al. [6] experimentally investigated the impact of foam filler on the compressive response

Technical Editor: João Marciano Laredo dos Reis.

✉ Amin Farrokhbadi  
amin-farrokh@modares.ac.ir

<sup>1</sup> Department of Mechanical Engineering, Tarbiat Modares University, Tehran, Iran

<sup>2</sup> Graduate Center, Aeronautical University of Science and Technology, Tehran, Iran

of hexagonal aluminum honeycomb structures under axial load. Zarei Mahmoudabadi and Sadighi [7] investigated the impact of using foam fillers on static and dynamic response of honeycomb hexagonal structures, using the theoretical as well as experimental approaches. The theoretical model for calculating the MCS of the foam-filled metal hexagonal honeycomb exposed to quasi-static loading conditions was provided using the energy method and accounting for the interaction effects between cell walls of honeycomb structures and foam filler. Sadighi and Salami [8] studied the low-velocity impact response generated by elastomeric and crushable foams. They initially put these foams under the quasi-static test, and then put them under the load of the low speed of the dynamical collapse of the hammer, and the numerical solution of this material was obtained under low-speed loading. Liu et al. [9] examined the axial and lateral crushing behavior of EPP foam-filled aluminum honeycomb structures. Through an experimental investigation, they aimed at exploring the impact of expanded polypropylene foam filler on the mechanical behavior of aluminum honeycomb panels. Zhang et al. [10] conducted an experimental and numerical investigation of aluminum honeycomb structures once filled with EPP foam (Expanded polypropylene). The findings showed that the initial peak strength as well as the mean strength of the filled honeycomb significantly increased, which is attributed to the interaction impact between the aluminum honeycomb wall and the foam filler; however, there was reduction in the specific energy absorption (SEA). Axial and oblique impact crash tests were conducted on hollow and honeycomb-filled aluminum square tubes in a study by Zarei and Kroger [11]. Multi-design optimization (MDO) technique was used to achieve the highest energy/specific EA of square, rectangular and circular tubes. In last few decades, there has been numerous research on thin-walled metal structures filled with foam and honeycomb. Santosa [12] conducted a study on the crushing behavior of columns filled with foam or aluminum honeycomb. Kılıçaslan [13] implemented a numerical crushing analysis on aluminum foam-filled corrugated single- and double-circular tubes under axial impact loading. In another study, Hussein et al. [14] investigated the crushing response of square aluminum tubes using polyurethane foam and aluminum honeycomb fillers. Yang et al. [15] examined the impact of foam fillers on the transition collapse mode of thin-walled circular columns once exposed to axial compression load using analytical, numerical and experimental approaches. A study by Zarei and Kröger [16] aimed at optimizing various parameters of aluminum honeycomb and foam-filled square and circular aluminum tubes exposed to dynamic impact loading.

In recent decades, designers have become very interested in using thin-walled composite structures in numerous applications, as well as energy-absorbing devices because of their

low weight and excellent crashworthiness [17]. The behavior of composite tubes in EA has been studied in many published articles [18, 19]. Mamalis et al. [20] presented an analytical model for composite conical tubes made of glass fiber under dynamic and static axial collapse loads. They compared the analytical model with experimental tests to empirically validate the model. Mehdi et al. [21] conducted a nonlinear finite element model for the analysis of the axially crushed cotton fiber composite corrugated tubes. Zarei et al. [22] performed the experimental and numerical crashworthiness investigations of thermoplastic composite crash boxes and verified the results of numerical model with the empirical findings. McGregor et al. [23] conducted a finite element analysis for the progressive crushing of braided composite tubes subjected to axial impact. Zhang et al. [24] analyzed the crashworthiness exploration of kagome honeycomb sandwich cylindrical column subjected to axial crushing load conditions. This novel device for absorbing the impact energy was created by two circular aluminum tubes filled with a core shaped as a large-cell kagome lattice. Niknejad et al. [25] investigated the momentary folding force of the polyurethane foam-filled square honeycombs via theoretical and experimental studies. Feraboli et al. [26] employed LS-DYNA MAT54 material model to investigate the axial crushing of a composite tape sinusoidal sample. Kathiresan et al. [27] performed an investigation on crashworthiness study of glass fiber/epoxy thin-walled composite conical frusta under axial compression. Via an observational analysis technique as well as a theoretical procedure, Boria et al. [28] made predictions on the post-collapse compression load of the composite shells. The obtained results were compared with the experimental results available from the literature. Siromani et al. [29] used a finite element analysis to determine the crushing response and EA capability of graphite/epoxy laminated circular tubes. Boria et al. [30] proposed a mathematical approach on the failure as well as stable modes of collapse of thin-walled composite structures under axial loading. To this end, the energy used for absorption was determined. Taking fiber orientation errors into account, Hwang et al. [31] analyzed the mechanical characteristics of conical composite tubes subjected to static loads. Also, they performed parametric studies on the effects of taper angles, sizes, and stacking sequences. Sun et al. [32] experimentally analyzed the crashing characteristics of aluminum/CFRP tubes exposed to axial and oblique loading. The failure modes, load–displacement diagrams, crushing force, and EA of all samples were determined, and the impact of loading angle was investigated.

Recently, attention to the application of thin-walled composite structures filled with foam and honeycomb has been increased. Sun et al. [33] conducted several quasi-static axial experiments and examined the crushing behavior of circular CFRP-aluminum-steel tubes with/without cellular

fillers and reported that the folding deformation of filled samples, i.e., foam/honeycomb was more stable than that of the empty samples. Nianfi et al. [34] investigated the EA of thin-walled aluminum structures filled with aluminum foam and polymer composites reinforced with carbon fibers filled with polyurethane foam. Experimental findings showed that CFRP tubes possessed a better EA capacity than aluminum alloy tubes. They concluded that the EA of circular CFRP tubes filled with PU foam was more desirable than the square and hexagonal structures. Elahi et al. [35] presented an analytical relationship for empty and filled polyurethane foam composite tubes exposed to lateral compressive load and compared the results obtained from the analytical relationships with the experimental outcomes. Zhang et al. [36] examined the dynamic and static crushing response of CFRP sandwich panels filled with various reinforcing materials. Zhou et al. [37] investigated the EA of composite tube reinforced by PVC foam cores for application in lightweight sandwich panels with desirable resistance. Mahbod and Asgari [17] performed analyzed the EA capability of a recently developed foam-filled corrugated composite tube subjected to axial and oblique loadings. Meriç and Gedikli [38] performed multi-objective optimization of the energy-absorbing behavior of foam-filled hybrid composite tubes. Yao et al. [39] presented a bio-inspired foam-filled multi-cell structural configuration for EA. Wang et al. [40] investigated foam-filled lightweight braided-textile reinforced and nested tubular structures for EA applications. Yao and et.al [41] conducted an experimental and numerical study on the EA of polyurethane foam-filled metal/composite hybrid structures. Lykakos et al. [42] performed a comparative experimental study of aluminum, GFRP, and hybrid aluminum/GFRP circular tubes under quasi-static and dynamic axial loading conditions. Parametric study on the crushing performance of a polyurethane foam-filled CFRP/Al composite sandwich structure performed by Yang et al. [43].

Due to the increasing use of fillers in thin-walled structures in recent years, a challenge that designers always face is the impact of these fillers on the crashworthiness characteristics and collapse of these structures. Reviewing the before mentioned studied, and as far as the authors are aware, so far, studies on the axial crashing behavior of *cylindrical composite tubes* filled with *both polyurethane foam and aluminum honeycomb* have not been conducted.

This work aims at exploring the crashworthiness characteristics of four cases including cylindrical hollow composite tubes, aluminum honeycomb-filled tubes, polyurethane foam-filled tubes, and polyurethane foam/aluminum honeycomb-filled cylindrical composite. These cylindrical structures are exposed to quasi-static load at a 5-mm/min constant strain rate by employing a 150 kN universal testing machine. The differential impacts of honeycomb, polyurethane foam polyurethane foam/honeycomb filling, and diameter and

thickness of wall of cylindrical composite are also investigated. Deformation mode, PCF, MCF, SEA as well as EA of the above structural compositions are also determined. Afterward, the mean crushing force of these cylindrical structures obtained analytically. Finally, a comparison is made between the findings of analytical mean crushing force and the experimental results. It should be noted that, for convenience, in the subsequent sections, aluminum honeycomb was the abbreviated from of "honeycomb" throughout the text and "H" in the tables and figures. Similarly, "foam" was used as the abbreviated from of Polyurethane throughout the text and "F" in the tables and figures. "Tube" represents cylindrical composite tubes throughout the text and "CCT" in the tables and figures.

## 2 Analytical modeling

This section presents details on the failure mechanisms related to the steady-state of collapse (Mode I) for thin-walled composite cylindrical tubes filled with foam and honeycomb subjected to quasi-static compression loading. These relations are used to make predictions on the mean loads and total displacements during collapse. The internal dissipated energy of the thin-walled composite cylindrical tubes filled with foam and honeycomb is determined as:

$$E_T = E_{SH} + E_H + E_F \quad (1)$$

where  $E_T$  is the absorbed energy by the whole system,  $E_{SH}$  is the absorbed energy by the cylindrical composite tube,  $E_H$  is the absorbed energy by the honeycomb, and  $E_F$  is the energy absorbed by the foam. In the subsequent section, the energy absorbed by each component is discussed.

### 2.1 Composite shell

While crushing a composite cylindrical structure under quasi-static compression loading, following the initial peak force, the oscillation of force happens around a mean force  $P$ . The initial marked reduction in the force results from the creation of a main circumferential interwall crack with height  $h$  at the upper-end parallel to the axis of the shell wall. While the deformation continues, at the same time, the outer petals formed bend down along the perimeter of the shell. Then several axial splits are followed by splaying of the material strips. Due to the bending damage that leads to the post-crushing regime, two groups of lamina bundles formed that bent inwards and outwards. It is worth noting that these lamina bundles resist against the applied force and buckle once the force or the length of the lamina bundle attains a critical amount. A triangular debris wedge of pulverized material is created at this moment. The formation of wedge may be assigned to the

friction created between the rigid platen and the bent bundles. It is worth considering that, in the current study, only the first cycle of progressive crushing is addressed, and the total deformation is achieved by repetitive continuous cycles possessing an identical pattern. Figure 1 shows the idealized model of the crush zone, where  $T$  is the shell thickness,  $\varphi$  the slope in the degree,  $R$  the mean radius, and  $H$  the axial height of the tube.

For simplicity of the deformation processes, some assumptions were made: the inwards and outwards petal sustain a constant length equal to  $h$ ; the transition between straightening and the bent zone is sudden, hence, the middle crack is set in A; due to the low level of the elastic energy, there was no focus on the elastic energy level with the first impact phase. EA involves four major modes throughout the creation of crush zone during the crushing process of composite tubes [44]: work needed for bending of fronds ( $W_b$ ), work needed for frond formation ( $W_h$ ), work needed for circumferential delamination ( $W_c$ ) and energy released as a result of friction between the debris wedge and petals and between petals and rigid platen ( $W_f$ ). The sum of the bending energy, the hoop energy, the energy needed for circumferential delamination, and friction energy yields the total energy release due to the deformation of the shell:

$$W_t = W_b + W_h + W_c + W_f \tag{2}$$

This total dissipated energy equals the work performed by the external force  $P$  on the crushing displacement  $\delta$  in a single progression, i.e.

$$W_e = P\delta = Ph[\cos\varphi - \cos(\alpha - \varphi)] \tag{3}$$

The function of the mean force  $P$  is a function of three variables of  $h, t_1, \alpha$ , depending upon three geometric parameters of  $\varphi, R$  and  $T$ , i.e.

$$P(h, t_1, \alpha; \varphi, R, T) = \frac{\pi}{(1 - \mu_1)h(\cos\varphi - \cos(\alpha - \varphi))} \left[ \frac{1}{3}\sigma_0 d_c (\alpha(t_1^2 + (T - t_1)^2) - 2\varphi t_1^2) + 2hGd_c + \sigma_0 h^2(T(\sin(\alpha - \varphi) + \sin\varphi) - 2t_1 \sin\varphi) + 4\sigma_0 h^2(\cos\varphi - \cos(\alpha - \varphi)) d_c(\mu_2 - \mu_1 \sin(\alpha - \varphi) - \mu_1 \mu_2 \cos(\alpha - \varphi)) \right] \tag{4}$$

where  $t_1$  and  $t_2$  are the thickness of the bended layers in the inwards and outwards directions of the shell radius,  $\alpha$  and  $\beta$  are the bending angles,  $\sigma_0$  is the ultimate stress in uni-axial tension of the composite laminate,  $G$  is the critical strain energy release rate per unit interlaminar delaminated crack area,  $\mu_1$  is the coefficient of friction between petal and rigid platen,  $\mu_2$  is the coefficient of friction between the wedge and the petals and  $d_c$  verifies as

$$d_c = R - \frac{T}{2} + t_1 + h \sin\varphi \tag{5}$$

### 2.2 Honeycomb and foam

Since foam-filled hexagonal honeycomb possesses a regular and symmetrical geometry, it is regarded as a structure with folding elements and two angular elements, assembled using an adhesive and foam filler surrounding these angular elements (Fig. 2). The average crushing force needed for the folding of the honeycomb with foam filler is determined using the energy method, which assumes that the dissipated energy equals the external work. The current position of the angular elements may be regarded as similar to the angular elements of a hollow honeycomb by considering the concertina mode as the folding mode of foam-filled honeycomb.

Put differently, the instantaneous position of the angular elements is assumed to be similar to the folding mode of

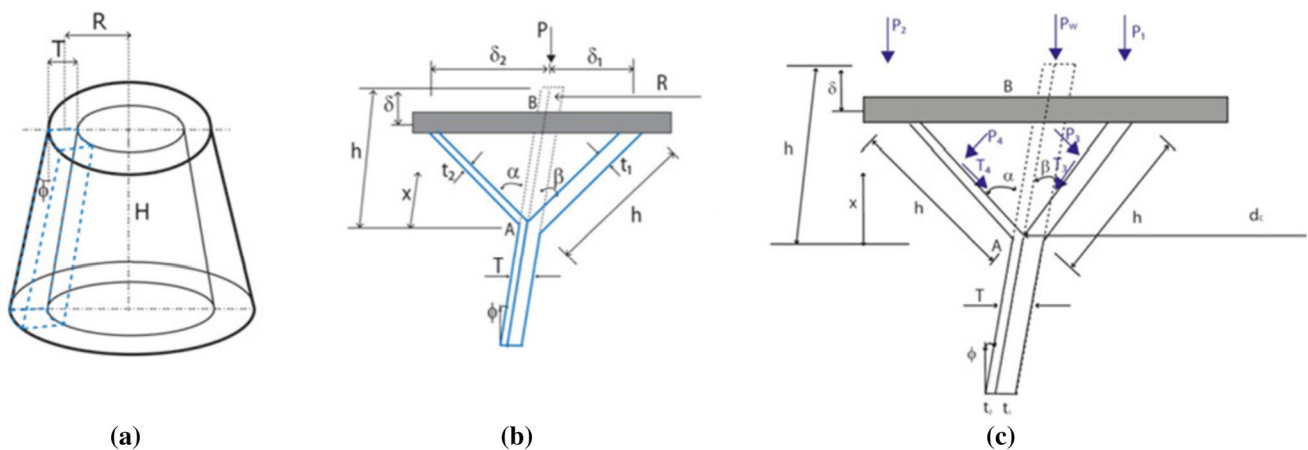


Fig. 1 Schematic of conical composite tube: **a** Shell prior to loading, **b** the ideal configuration of crushing zone, **c** the model of force [30]

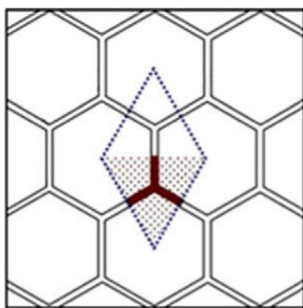


Fig. 2 Folding element of foam filled hexagonal honeycomb [7]

the hollow honeycomb angular elements, while the foam filler determines their final position. Figure 3 displays the global collapse mode of the hollow honeycomb angular element, reported by Wierzbicki. It includes (a) four-plane trapezoidal elements movement as rigid bodies, (b) two parts of cylindrical surfaces that possess an inextensional mode and only absorb the energy needed for the formation of two moving plastic hinges located upper and lower them, (c) two parts of conical surfaces bonded by two propagating straight hinge lines, and (d) a part of a toroidal shell which experiences an expansion [2].

The folding element yields the internal dissipated energy, which falls into two types: the internal energy term released from the deformation of honeycomb cell walls  $E_h$  and the internal energy term released from the plastic deformation of the foam filler,  $E_f$ . In other words, the crushing process of the honeycomb cell walls yields three types of energy: (a) the energy wasted during the expansion of the toroidal shell,  $E_1$ , (b) the energy wasted by forming the horizontal plastic hinge lines of the cylindrical surfaces,  $E_2$ , and (c) the energy released by forming of inclined plastic hinge lines of the conical parts,  $E_3$ . So,

$$E_H = E_1 + E_2 + E_3 \tag{6}$$

Referring Figs. 3 and 4, three internal dissipated energy terms while crushing honeycomb cell walls are identified as [2]:

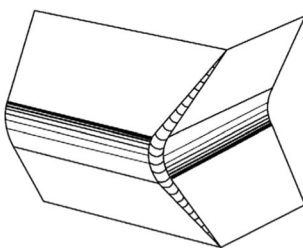


Fig. 3 The collapse mode of an angular element [7]

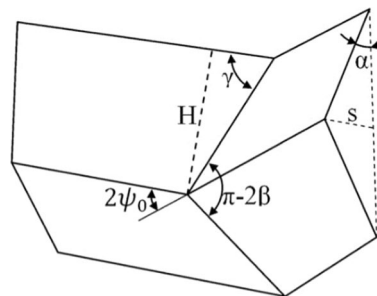


Fig. 4 The geometry of the folding mode of an angular element [7]

$$E_1 = 32M_0 \frac{Hb}{h} I_1(\psi_0) \tag{7a}$$

$$E_2 = 12M_0 D \alpha^* \tag{7b}$$

$$E_3 = 8M_0 \frac{H^2}{b} I_3(\psi_0) \tag{7c}$$

Thus, crushing of the honeycomb cell walls results in the dissipation of the internal energy which can be evaluated as

$$E_H = M_0 \left[ 32 \frac{Hb}{h} I_1(\psi_0) + 12D\alpha^* + 8 \frac{H^2}{b} I_3(\psi_0) \right] \tag{8}$$

where  $H$  is the half-wavelength of the folding mode,  $b$  is the small radius of the toroidal shell,  $D$  is the thickness of the cell wall,  $h$  represent its width,  $M_0$  shows the fully plastic bending moment, and  $2\psi_0$  is the angle between the two adjoining plates, once viewed normal to the plane of the honeycomb. Furthermore,  $\alpha^*$  is the final value of the angle  $\alpha$ , indicated in Fig. 4.  $I_1(\psi_0)$  and  $I_3(\psi_0)$  are functions of  $\alpha^*$ .

Three separated zones construct the stress–strain diagram of crushable foam. They include elastic zone, plateau zone, and densification zone. The crushing process of the foam yields the internal energy dissipated [7]

$$E_f = \frac{\sqrt{3}}{2} \sigma_f^* \epsilon_f^* S^2 H \tag{9}$$

$\sigma_f^*$ , is flow stress of the foam,  $\epsilon_f^*$  is its densification strain, and  $S$  is the cell size.

The external work needed for the formation of a single fold in the folding element can be expressed as

$$E_{ext} = P_m \delta \tag{10}$$

The total internal energy dissipation associated with the folding element equals the external work. Hence, the mean crushing force is calculated [7]:

$$P_m = \frac{1}{2H - 2((H - b\alpha^*) \cos \alpha^* + b \sin \alpha^*)} \left\{ M_0 \left[ 32 \frac{Hb}{h} I_1(\psi_0) + 12D\alpha^* + 8 \frac{H^2}{b} I_3(\psi_0) \right] + \sigma_f^* \epsilon_f^* \frac{\sqrt{3}}{2} S^2 H \right\} \tag{11}$$

When the foam filler strain is equal to the strain at which densification is initiated in the foam, persisting of the foam crushing gets complicated. To determine  $\alpha^*$  which is the final value of  $\alpha$ , we assume that the crushing process stops at the foam densification strain,  $\epsilon_f^*$ . The foam densification strain is determined as

$$\epsilon_f^* = 1 - \left\{ \left( 1 - \frac{b}{H} \alpha^* \right) \cos \alpha^* + \frac{b}{H} \sin \alpha^* \right\} \tag{12}$$

The final value of the angle  $\alpha$ ,  $\alpha^*$ , is calculated in terms of  $H$ ,  $b$  and  $\epsilon_f^*$  by solving Eq. (12). Once the angle  $\alpha^*$  is identified, the unknown parameters for determining  $P_m$  in Eq. (11) are  $H$  that represents the half-wavelength of the folding mode and  $b$ , which is the small radius of the toroidal shell. The minimum achievable value of the average crushing force resulting in collapse is determined by:

$$\begin{aligned} \frac{\partial P_m}{\partial H} &= 0 \\ \frac{\partial P_m}{\partial b} &= 0 \end{aligned} \tag{13}$$

Substituting  $P_m$  from Eq. (11) into (13) results

$$\begin{aligned} \frac{\partial P_m}{\partial H} &= \left\{ \frac{1 - \cos \alpha^*}{2[H - ((H - b\alpha^*) \cos \alpha^* + b \sin \alpha^*)]^2} \right\} \\ &\left\{ M_0 \left[ 32 \frac{Hb}{h} I_1(\psi_0) + 12D\alpha^* + 8 \frac{H^2}{b} I_3(\psi_0) \right] \right. \\ &\left. + \sigma_f^* \epsilon_f^* \frac{\sqrt{3}}{2} S^2 H \right\} + \frac{1}{2H - 2((H - b\alpha^*) \cos \alpha^* + b \sin \alpha^*)} \\ &\left\{ M_0 \left[ 32 \frac{b}{h} I_1(\psi_0) + 16 \frac{H}{b} I_3(\psi_0) \right] + \sigma_f^* \epsilon_f^* \frac{\sqrt{3}}{2} S^2 \right\} = 0 \end{aligned} \tag{14}$$

$$\begin{aligned} \frac{\partial P_m}{\partial b} &= \frac{\alpha^* \cos \alpha^* - \sin \alpha^*}{2[H - ((H - b\alpha^*) \cos \alpha^* + b \sin \alpha^*)]^2} \\ &\left\{ M_0 \left[ 32 \frac{Hb}{h} I_1(\psi_0) + 12D\alpha^* + 8 \frac{H^2}{b} I_3(\psi_0) \right] \right. \\ &\left. + \sigma_f^* \epsilon_f^* \frac{\sqrt{3}}{2} S^2 H \right\} + \frac{1}{2H - 2((H - b\alpha^*) \cos \alpha^* + b \sin \alpha^*)} \\ &\left\{ M_0 \left[ 32 \frac{H}{h} I_1(\psi_0) - 8 \frac{H^2}{b^2} I_3(\psi_0) \right] \right\} = 0 \end{aligned} \tag{15}$$

Solving Eqs. (14) and (15) gives the values or the unknown parameters simultaneously. To this end, an initial

guess for  $H$  and  $b$  is made. Once the values for  $H$  and  $b$  are substituted into Eq. (12), and it is solved for a specified value of  $\epsilon_f^*$ , results a value for  $\alpha^*$  is obtained. By obtaining  $\alpha^*$ , the parameters  $I_1(\psi_0)$  and  $I_3(\psi_0)$  can be found. By replacement of the assumed values of  $H$ ,  $b$  and the obtained values for  $\alpha^*$ ,  $I_1(\psi_0)$  and  $I_3(\psi_0)$  into Eqs. (14) and (15) and drawing on a numerical approach, the new values for  $H$  and  $b$  are derived. Repetition of this cycle by employing the calculated values of  $H$  and  $b$  as a new guess yields the constant values for  $H$  and  $b$ . Then, the mean crushing force,  $P_m$ , can be attained by the replacement of the constant values of  $H$  and  $b$  into Eq. (11).

### 3 Experimental

#### 3.1 Materials properties

##### 3.1.1 Cylindrical composite tube

All samples were fabricated by E-glass fiber plane woven (MW-200) and polyester resin using winding process. First, the E-glass fiber plane woven was impregnated with polyester resin. After that, the prepregs were cut into rectangular plies. Two cylindrical steel molds with approximate diameters of 40 and 50 mm were used to make cylindrical composite tubes. To easily remove and decrease the surface friction to facilitate the tube demolding, the surface of the steel mold was cleaned with soft sandpaper, and a layer of silicone spray was sprayed on the mold, after which the silicone spray and the steel mold were impregnated with a layer of wax (shown in Fig. 5). Then the machine started to rotate the steel mold with a suitable rotational speed and E-glass fiber plane woven was wrapped around the mold with approximate thicknesses of 1.5, 2 and 3 mm. To obtain the wall thickness of composite tubes with a thickness of 1.5, 2, and 3 mm, 15, 20, and 30 layers of impregnated E-glass fiber plane woven with polyester were wrapped around the molds, respectively. The stacking scheme of the composite tubes with different thicknesses is shown in Fig. 5b. After the winding process, a long composite tube was cured at 90 °C for five hours. Subsequently, the cured tube was demolded from the steel molds (illustrated in Fig. 6a) and waited for post-processing, where it was cut for a required length by the saw cut. The length of all samples was 80 mm with approximate diameters of 40 and 50 mm and a wall thickness of 1.5, 2 and 3 mm.

To establish the mechanical characteristics of the composite tubes, tensile tests were performed based on the ASTM D3039 standard [45]. The tensile samples were fabricated by hand lay-up method and were cured at 90 °C temperature for five hours. Three tensile coupons (Fig. 7a) were prepared using a water jet machine. Tensile tests were



**Fig. 5** a Preparation of the cylindrical composite tube, b The stacking scheme of the composite tubes with different thicknesses

**Fig. 6** a Cylindrical composite tube cut with wire cut, b cylindrical composite tube filled with both foam and honeycomb

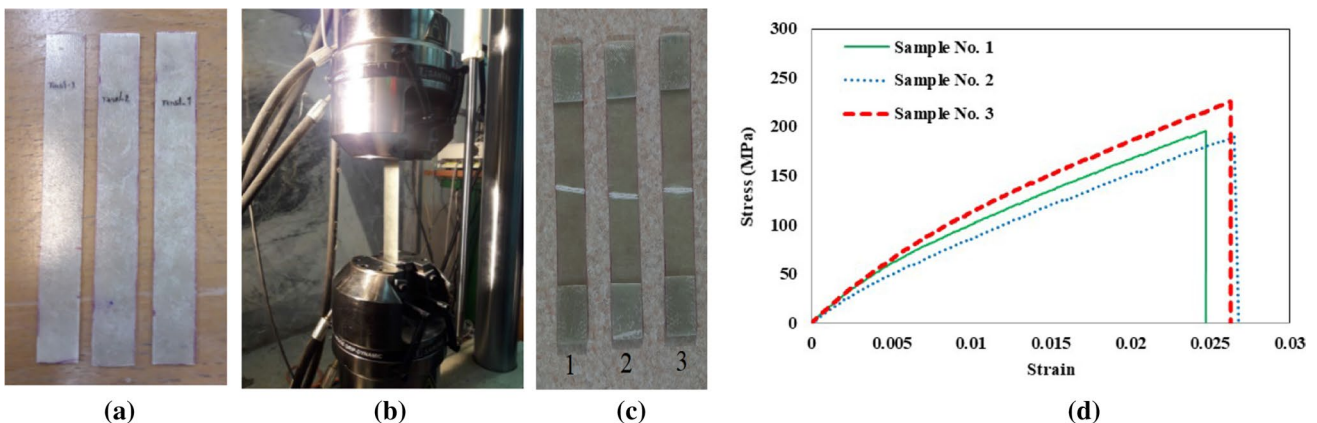


**Fig. 7** a Three tensile coupons, b the sample under tensile test, c the sample after the tensile test, d stress–strain diagrams of composite coupon tests

performed using a 50 kN SANTAM testing machine at a 1-mm/min constant strain rate. Figure 7b indicates a typical tensile coupon testing. The tensile tests were performed at the ambient temperature of 23 °C according to ASTM D 3039 standard. The samples after the tensile test were shown in Fig. 7c. The mode and location code of failure of the samples were angled gage middle (AGM) according to ASTM D 3039 standard. Engineering stress–strain diagrams of composite coupon tests were shown in Fig. 7d.

### 3.1.2 Aluminum honeycomb

A Hex Web® CR III aluminum alloy 5052 with an H39 temper was used to make the honeycomb. Wire cut was used to prepare the honeycomb in a cylindrical shape shown in Fig. 8a, b. An image of a typical cylindrical honeycomb sample was displayed in Fig. 8c, with 40 mm diameter and height of 40 mm. This type of honeycomb possesses the nominal density, cell size and cell wall thickness of

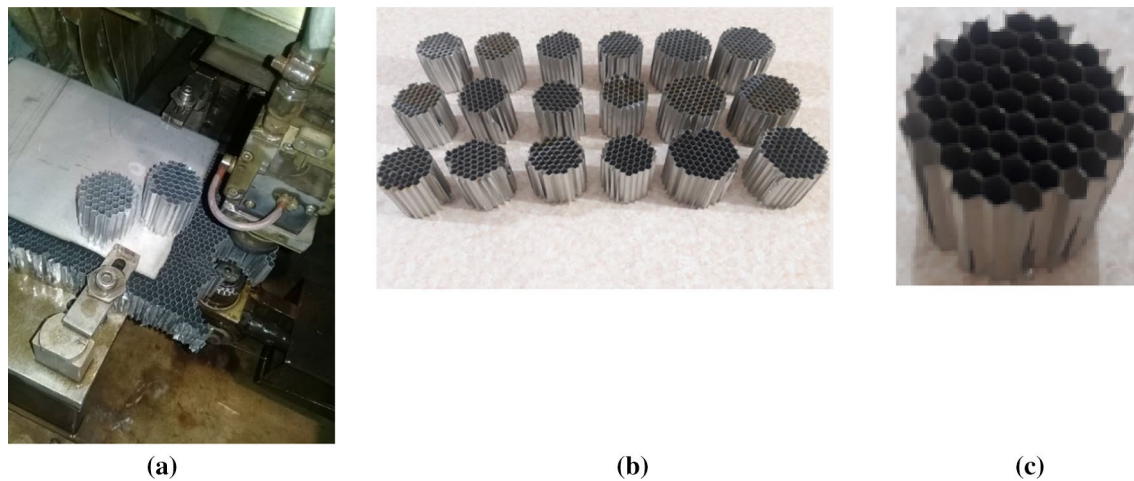


**Fig. 8** **a** Honeycomb sample preparation by wire cut; **b** cut aluminum honeycomb with different diameters; **c** typical cylindrical honeycomb sample with 40 mm diameter and a height of 40 mm

**Table 1** Aluminum honeycomb, foam, and foam-filled aluminum honeycombs specifications

Sample	Aluminum honeycomb		Foam
	Wall thickness (mm)	Cell size (mm)	Foam density (kg/m <sup>3</sup> )
H40-1	0.0508	4.687	–
H40-2	0.0508	4.687	–
HF40-1	0.0508	4.687	55
HF40-2	0.0508	4.687	55
F40-1	–	–	55
F40-2	–	–	55
F50-1	–	–	–
F50-2	–	–	55

49.657 kg/m<sup>3</sup>, 4.687 mm and 0.0508 mm, respectively, as shown in Table 1. Figure 9a illustrates a typical quasi-static compression testing of honeycomb. The stress–strain diagrams of this type of honeycomb crashed at the constant strain rate 5 mm/min was shown in Fig. 9b. The plateau stress of the honeycomb was 1.11 MPa.

### 3.1.3 Polyurethane foam

In the current research, polyurethane foam with an approximately density of 55 kg/m<sup>3</sup> was applied to increase the strength of the honeycomb and cylindrical tubes. The polyurethane foam applied in this research is an eco-compatible foam with two chemical elements (Isocyanate and Polyol). To achieve the desirable density of this foam, its constituent elements were combined in a weight ratio of 1:1. Subsequently, the foam is injected and cured inside a

cylindrical mold with a 40-mm inner diameter and a 100-mm height (Fig. 10a). Foam density was calculated drawing upon ASTM D1622/D1622M standard [46]. Quasi-static compression tests of polyurethane samples were performed drawing on the ASTM D1621 standard [47] at the strain rate of 5 mm/min. All samples illustrated in Table 1 were crushed up to 85% of their initial lengths, and to validate the results, the quasi-static test was run four times. Figure 10b shows the stress–strain diagram of samples. Plateau stresses were also determined as the mean stresses from a strain of 0.05–0.6 and appeared to be 0.42 MPa at the constant strain rate of 5 mm/min.

### 3.2 Preparing the test sample

The samples of this research fall into four groups, as shown in Table 2 and Fig. 6b. Their initial length was 80 mm. The first group was cylindrical composite tubes (CCT). The second group included aluminum honeycomb-filled cylindrical composite tubes (CCTH). Two similar honeycomb parts, which were 40 mm long, were inserted inside cylindrical composite tubes with a length of 80 mm. The third group included polyurethane foam-filled cylindrical composite tubes (CCTF). A hand mixer at 1000 rpm was applied to mix the two constituents of this foam (Isocyanate and Polyol) at a weight ratio of 1:1 for 15 s. Then, during the cream time (23 s), the mixture was poured in the tube. A sticky tape sealed one of the tube ends. This foam enjoys an expansion rate of 5 times the poured foam volume (that was almost 20% of the tube length), which expands to fill the cylindrical composite tube. The sample ends were cut and sanded after the foam was cured to eliminate additional polyurethane foam. The fourth group represented a novel structuring for increasing the strength of cylindrical composite tubes for which both polyurethane foam and



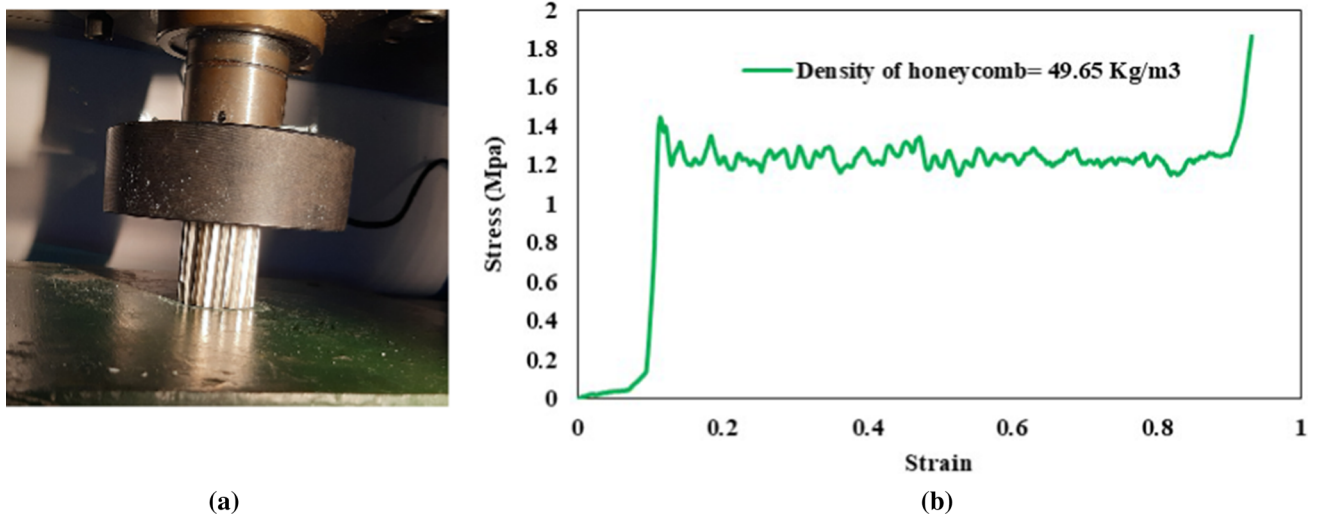


**Fig. 9** **a** A picture of an aluminum honeycomb sample; **b** stress–strain diagrams of honeycomb samples tested under the quasi-static compression load

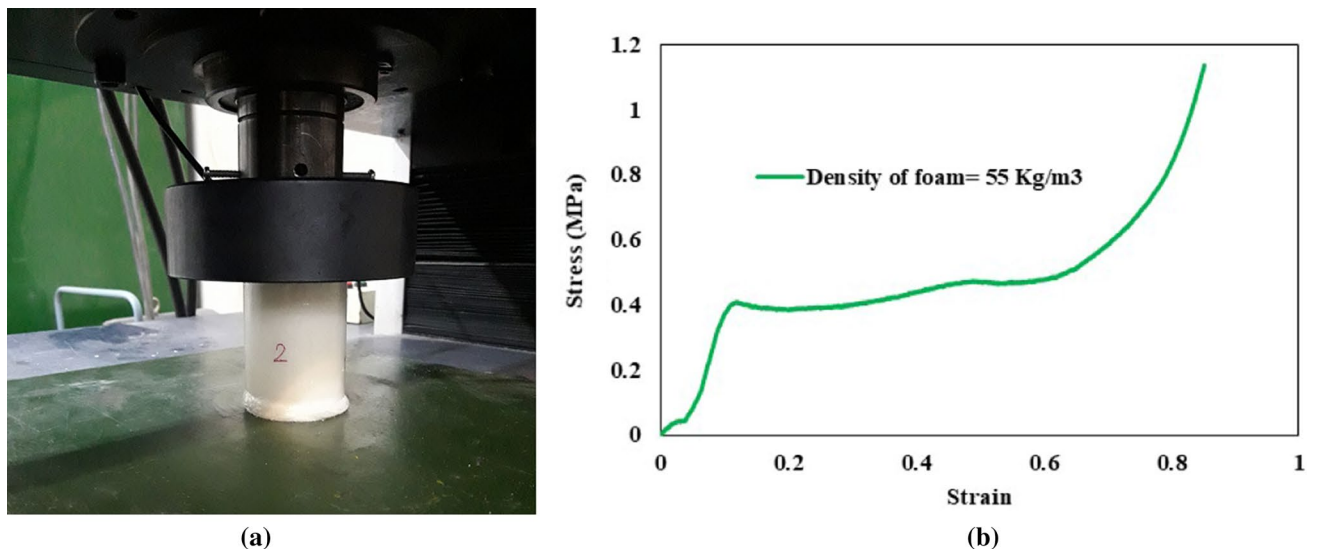


**Fig. 10** **a** A picture of a polyurethane foam sample; **b** stress–strain diagrams of polyurethane foam samples tested at the quasi-static compression load

aluminum honeycomb fillers were used (CCTHF). A similar procedure as in the third group was applied to prepare the samples in this group. Once the polyurethane foam mixture was poured, two similar honeycomb parts were quickly inserted inside the cylindrical composite tubes. The expansion of the foam was initiated until all honeycomb cells were filled with foam. Subsequently, the additional polyurethane foam at the ends of the samples was discarded. It should be noted that, for better realizing the samples, some code numbers are attributed to the composite shell samples. The first numbers, i.e., 40 and 50 that appear after the last letters in the sample, represent the diameter of the sample respectively. In addition, the first

numbers mentioned after the (–), i.e., 1, 2, and 3, refer to the wall thickness of cylindrical tube of 1.5 mm, 2 mm, and 3 mm, respectively, and the second number represents the repeated test.

## 4 Results and discussions

### 4.1 Quasi-static compression tests

Samples in all groups were subjected to quasi-static compression tests to investigate their collapse modes and attain

**Table 2** Sample groups and specifications

Group no.	Sample	Cylindrical composite tube				Aluminum honeycomb		Foam	Total weight (g)
		Diameter (mm)	Thickness (mm)	Mass (g)	Lengths (mm)	Wall thickness (mm)	Cell size (mm)	Foam density (kg/m <sup>3</sup> )	
1	CCT40-11	39.4	1.5	14.33	80	–	–	–	14.33
1	CCT40-12	39.4	1.5	14.88	80	–	–	–	14.88
1	CCT40-13	39.4	1.5	14.92	80	–	–	–	14.92
1	CCT40-14	39.4	1.5	14.96	80	–	–	–	14.96
1	CCT40-21	39.5	1.85	19.98	80	–	–	–	19.98
1	CCT40-22	40	1.85	20.27	80	–	–	–	20.27
1	CCT40-31	39.4	2.8	29.84	80	–	–	–	29.84
1	CCT40-32	39.5	2.8	29.84	80	–	–	–	29.84
1	CCT50-31	50	2.9	34.94	80	–	–	–	34.94
1	CCT50-32	50	2.9	34.94	80	–	–	–	34.94
2	CCTH40-21	39	1.9	20.63	80	0.0508	4.687	–	23.96
2	CCTH40-22	39	1.9	20.2	80	0.0508	4.687	–	23.40
3	CCTF40-11	39.4	1.4	14.37	80	–	–	55	18.35
3	CCTF40-12	39.4	1.4	14.32	80	–	–	55	18.20
3	CCTF40-21	39.6	1.9	19.13	80	–	–	55	23.05
3	CCTF40-22	40	1.9	19.77	80	–	–	55	23.69
3	CCTF40-31	39.6	2.8	30.63	80	–	–	55	34.59
3	CCTF40-32	39.6	2.8	32.07	80	–	–	55	35.98
3	CCTF50-21	50	1.8	24.71	80	–	–	55	30.46
3	CCTF50-22	50	1.8	24.71	80	–	–	55	30.46
3	CCTF50-31	50	2.9	35.90	80	–	–	55	41.25
3	CCTF50-32	50	2.9	35.90	80	–	–	55	41.25
4	CCTHF40-11	39.4	1.4	14.20	80	0.0508	4.687	55	24.08
4	CCTHF40-12	39.9	1.4	14.88	80	0.0508	4.687	55	24.56
4	CCTHF40-21	39	2	20.58	80	0.0508	4.687	55	29.87
4	CCTHF40-22	39.1	1.85	20.65	80	0.0508	4.687	55	29.62
4	CCTHF40-31	38.8	2.8	32.63	80	0.0508	4.687	55	43.27
4	CCTHF40-32	39	2.8	32.52	80	0.0508	4.687	55	41.29
4	CCTHF50-21	50	1.9	24.30	80	0.0508	4.687	55	39.78
4	CCTHF50-22	50	1.9	24.30	80	0.0508	4.687	55	39.78
4	CCTHF50-31	50	2.9	38.88	80	0.0508	4.687	55	52.74
4	CCTHF50-32	50	2.9	38.88	80	0.0508	4.687	55	52.74

their crash load–displacement diagrams, and finally the EA. A quasi-static compression load at the constant strain rate was applied by a 300 kN electronic microcomputer universal testing machine. A computer was attached to record the crashing load and displacement. Axial quasi-static compression load was applied for test samples at the constant strain rate of 5 mm/min. During the testing, while the lower platen was fixed, the upper platen of the machine moved downwards to crash the tubes. To ascertain about the consistency of the experimental findings, the quasi-static compression tests of hollow tube samples with

1.5 mm wall thickness were repeated four times (Fig. 11). The four load–displacement diagrams match very well. It should be noted that the difference between the CCT40-11 test data and the other three groups can be attributed to the test error such as the measurement error of the electronic microcomputer universal testing machine and etc. The remaining samples were subjected to tests two times under similar test condition. In the subsequent section, a representative crash load–displacement diagram for each test condition is displayed. Samples in all the experimental groups were crashed up to 80% of their initial lengths.

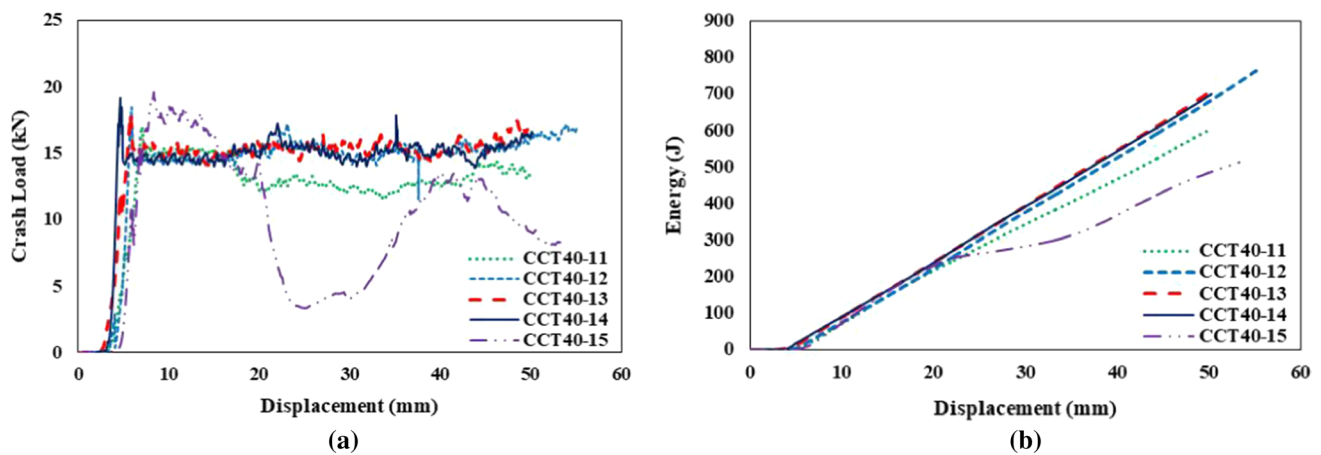


**Fig. 11** **a** Crash load–displacement diagrams for five repeated tests of the hollow cylindrical tube with 1.5 mm wall thickness; **b** energy-displacement diagrams for five repeated tests of the hollow tube with 1.5 mm wall thickness

## 4.2 Crashworthiness indicators

To evaluate the energy absorption capacity of structures, several criteria are commonly used in crashworthiness assessment. In this research, the magnitudes of crushing parameters are calculated directly from the crash load–displacement diagrams. Energy absorption (EA), peak crushing force (PCF), mean crushing force (MCF) and specific energy absorption (SEA) are frequently used as the important indicators for evaluating the crashworthiness. Peak crushing force (PCF) is defined as the first peak load. Energy absorption (EA) is the energy dissipated by the test specimens during the crushing process. It was determined from the area under the crash load–displacement diagrams can be calculated as:

$$EA = \int_{x=0}^{x=a} F(x)dx \quad (16)$$

where  $dx$  is the crushing distance and  $F(x)$  denotes the crushing force. The MCF for a given deformation can be expressed as:

$$MCF = \frac{1}{a} \int_{x=0}^{x=a} F(x)dx \quad (17)$$

Crushing force efficiency (CFE) is defined as the ratio of the mean crushing force (MCF) to the peak crushing force (PCF) of a structure can be calculated as:

$$CFE = \frac{MCF}{PCF} \quad (18)$$

The SEA is defined as the ratio of the absorbed energy to the mass of the structure. So it can be written as:

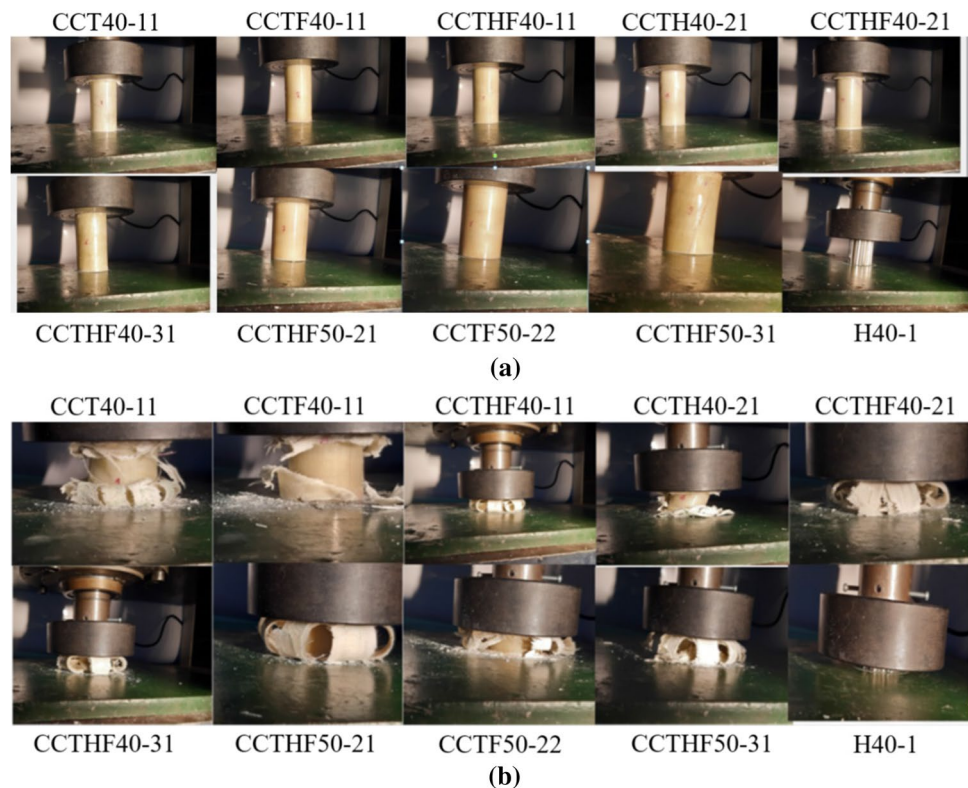
$$SEA = \frac{EA}{m} \quad (19)$$

where  $m$  represents the whole mass of the structure. The structure has good energy absorbing capacity when its SEA is high. It is worth noting that the value of crushing distance “ $a$ ” for foam-filled structures mainly depends on the crushing distance where the inner foam reaches the densification point. To compare the EA and SEA of different specimens in this experiment, we choose the same value of “ $a$ ”. Because the foam is earlier to reach densification, we determine the value of “ $a$ ” by referring to the crash load–displacement diagram of foam-filled structures and the “ $a$ ” is equal to 66 mm in this study.

## 4.3 Results of quasi-static compression tests

Each of the test groups underwent an axial quasi-static compression loading at the constant strain rate of 5 mm/min. The stable modes of collapse were observed for hollow tubes (Group 1) and CCTHF (Group 4) as demonstrated in Fig. 12. Hollow tubes (Group 1) and CCTHF (Group 4) yielded varied deformation modes compared to samples CCTH (Group 2) and CCTF (Group 3), as illustrated in Fig. 13. For the samples in group 1 and group 4, the outer petals formed bend down along the perimeter of the shell, of several axial splits followed by splaying of the material strips. The formation of two lamina bundles bent inwards and outwards as a result of the flexural damage occurred in the post-crushing regime (Fig. 14). Crash load–displacement diagrams for all tubes in this study are demonstrated in Fig. 15a–d. Energy absorb-displacement diagrams for all tubes are also illustrated in Fig. 16a–d. Table 3 shows the summary of PCF,

**Fig. 12** **a** Initial deformation of all group tubes under quasi-static load; **b** final deformation of all group tubes under quasi-static load



MCF, crushing force efficiency (CFE), EA, and SEA for all samples in all groups under study. Table 3 also shows the average values of MCF, CFE, EA, and SEA for the samples subjected to repeated tests.

#### 4.4 Effect of foam core on tubes

The use of foam as a filler in thin-walled tubes reduces the PCF and increases the CFE because it prevents the elastic instabilities of thin-walled tubes under axial compression load. Crash load–displacement and energy absorb–displacement diagrams for the tubes filled with foam are displayed in Figs. 15c and 16c respectively. As it is expected, the PCF, MCF, total EA, and CFE of foam-filled tubes exceed that of hollow tubes, and SEA of foam-filled tubes is smaller than that of hollow tubes because the solidity ratio of foam used in this study was low. According to the obtained results, EA and MCF of foam-filled tubes are 13.78% and 13.65% higher than the hollow tubes, respectively, at the same displacement of 66 mm. According to the obtained results, EA, SEA and MCF of foam-filled tubes are 7.95%, 9.24% and 7.98% higher than the honeycomb-filled tubes (Group 2) respectively at the same displacement of 66 mm with a 40-mm inner diameter and a 2-mm wall thickness. Also CFE of foam-filled tubes exceed that of honeycomb-filled tubes at the same displacement of 66 mm with a 40-mm inner diameter and a 2-mm wall thickness. Figure 13 indicates the collapse and deformation mode of tubes filled with foam

(Group 3) with a 40-mm inner diameter and a 1.5-mm wall thickness in the end-crushing mode (Mode I). While the collapse and deformation mode of foam-filled tubes (Group 3) with inner diameter 40 mm and wall thickness 2 and 3 mm is slightly different with foam-filled tubes (Group 3) with a 40-mm inner diameter and wall thickness of 1.5 mm. In the foam-filled tubes crush zone, external frond, circumferential crack, foam compaction, delamination, interlaminar delamination, and fragmentation of tube wall were observed that shown in Fig. 13. It should be noted that each of these failures causes energy absorption. For foam-filled tubes with a 40-mm inner diameter and 1.5-mm wall thickness, once PU foam is expanded outward during the compression, outward pressure is produced on the tubes shells, resulting in the formation of the external petal of the tubes shell.

The effect of foam on the crashworthiness characteristics and deformation of the failure mechanism depends on its density. Mahboob and Asghari [17] concluded that with increasing the density of the foam, the EA, MCF, and SEA of foam-filled tubes increase, while with increasing density of the foam, crushing length decreases.

#### 4.5 The impact of a combination of foam and aluminum honeycomb filling on tubes

According to the obtained results, the collapse mode of CCTHF is much more stable compared to other groups tubes, and they yield smoother crash load–displacement

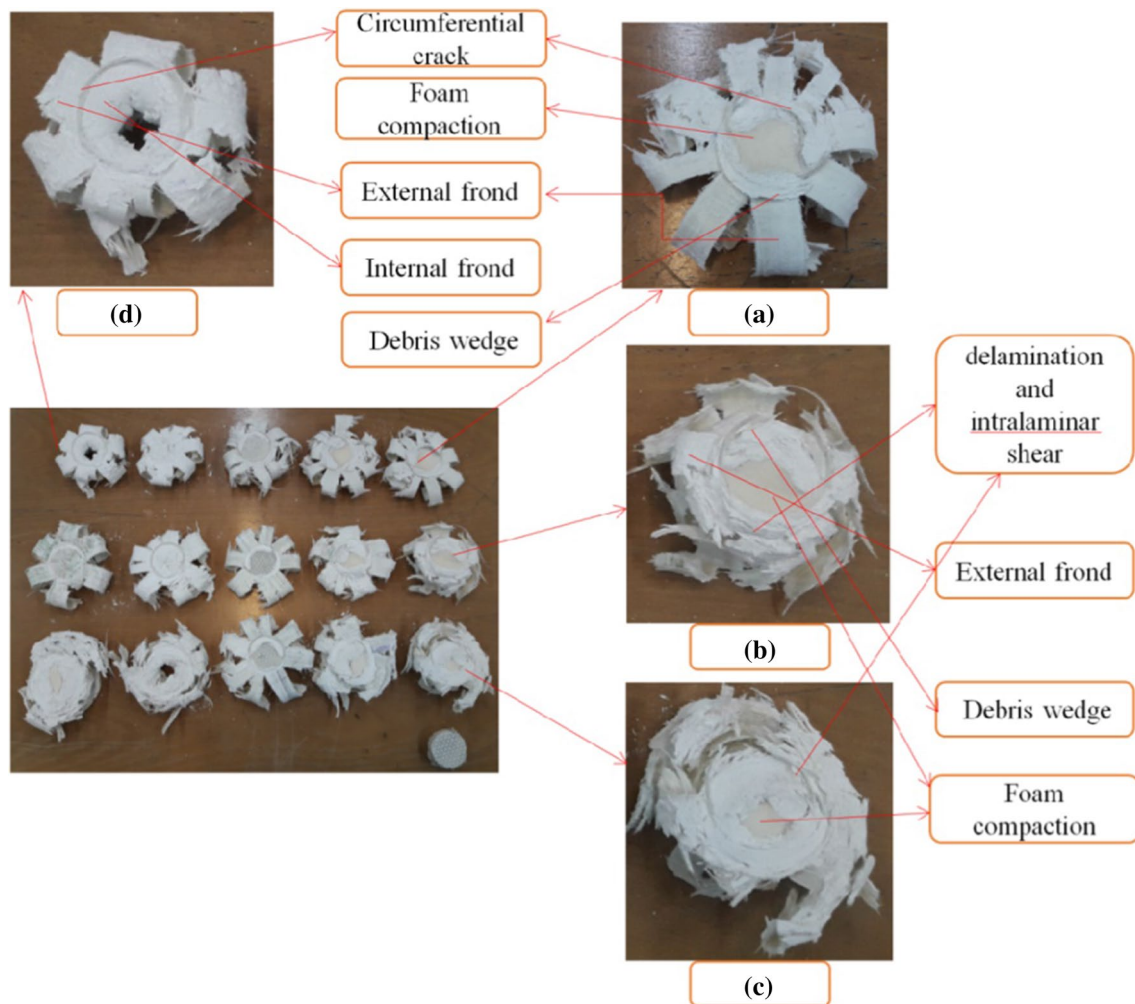


**Fig. 13** Deformation mode of foam-filled tubes; **a** with a 40-mm inner diameter and a 1.5-mm wall thickness; **b** with a 40-mm inner diameter and a 2-mm wall thickness; **c** with a 40-mm inner diameter and a 3-mm wall thickness; and **d** deformation mode of hollow tubes

diagrams compared to other groups tubes, suggesting that CCTHF tubes have superior balance of crushing stability than other groups of tubes. According to Mamalis et al. [20, 48] and the experimental observations of this study the major modes of failure fall into four categories:

- The end-crushing steady-state (Mode I) is characterized by the fragmentation of the composite material associated with a significant rate of fall energy, generally described by the steady collapse of the crust and the creation of continuous petals and/or a powdered triangular wedge;
- Transition failure due to longitudinal crack progression (Mode II) distinguished by the appearance of a crack propagating rapidly up from the bottom of the tube, resulting in an unstable global rupture of the shell;
- Circumference crack in the mid-length (Mode III) yielding catastrophic separation of the loaded shell

into two halves maintaining a limited deformation and yielding undesirable energy-absorbing properties;

- Progressive folding mode (Mode IV) is similar to the collapse of plastic and metal tubes.

Figure 14 shows that the collapse and deformation mode of all foam/honeycomb-filled tubes (Group 4) in the end-crushing mode (Mode I) compared to other groups tubes. In designing such structures, it is very important to predict the collapse mode and crushing behavior. Basically, it can be said the collapse and deformation of the tubes filled with both foam and honeycomb has a more predictable and stable crushing behavior than the tubes of other groups. For foam/honeycomb-filled tubes, once PU foam and honeycomb are expanded during the compression, outward pressure is applied on the outer tubes' shells, hindering denting, swelling, and flattening of the elastic outer tubes shells. As a result, a desirable axial



Fig. 14 Deformation mode of foam/honeycomb-filled tubes (Group 4)

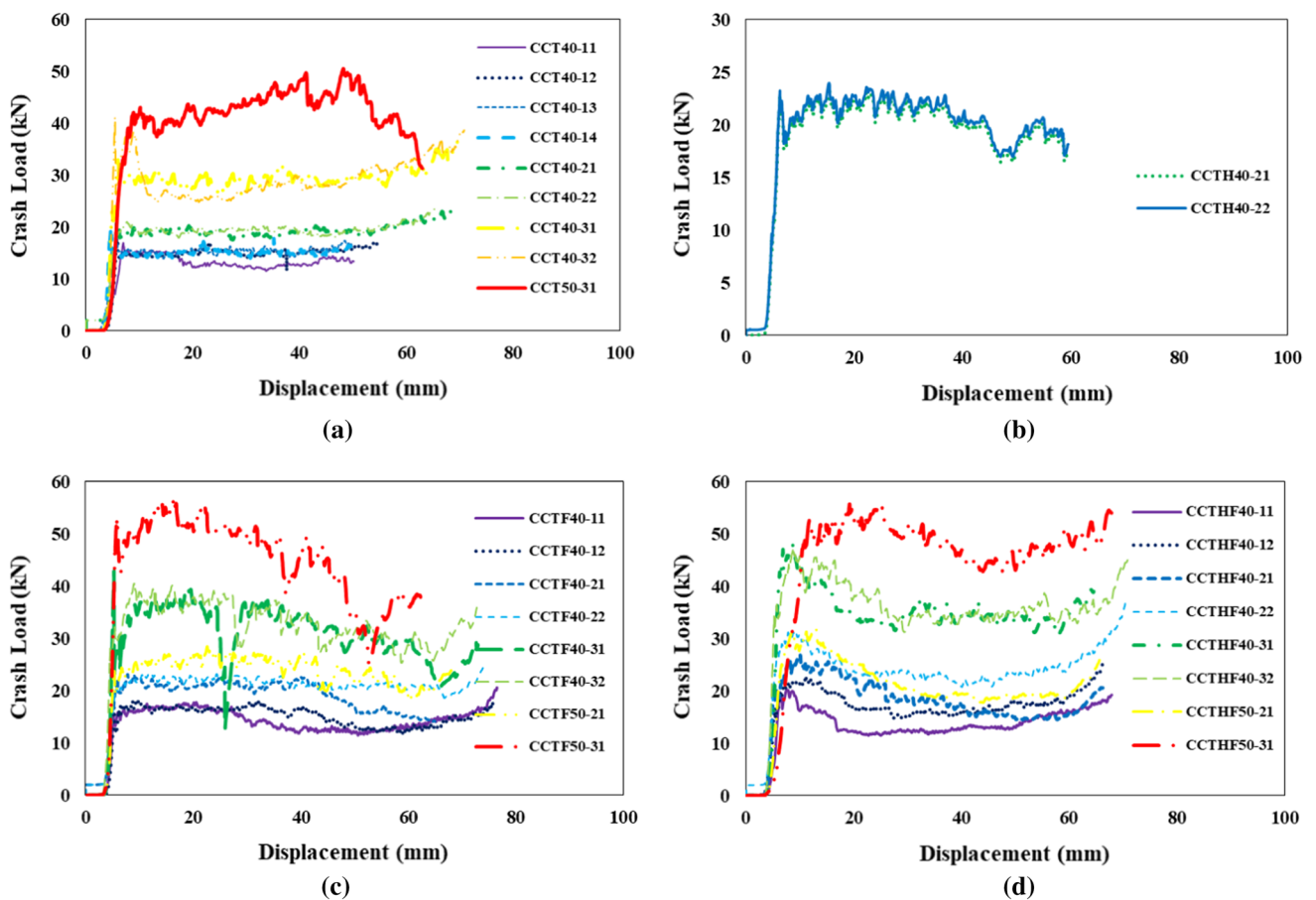
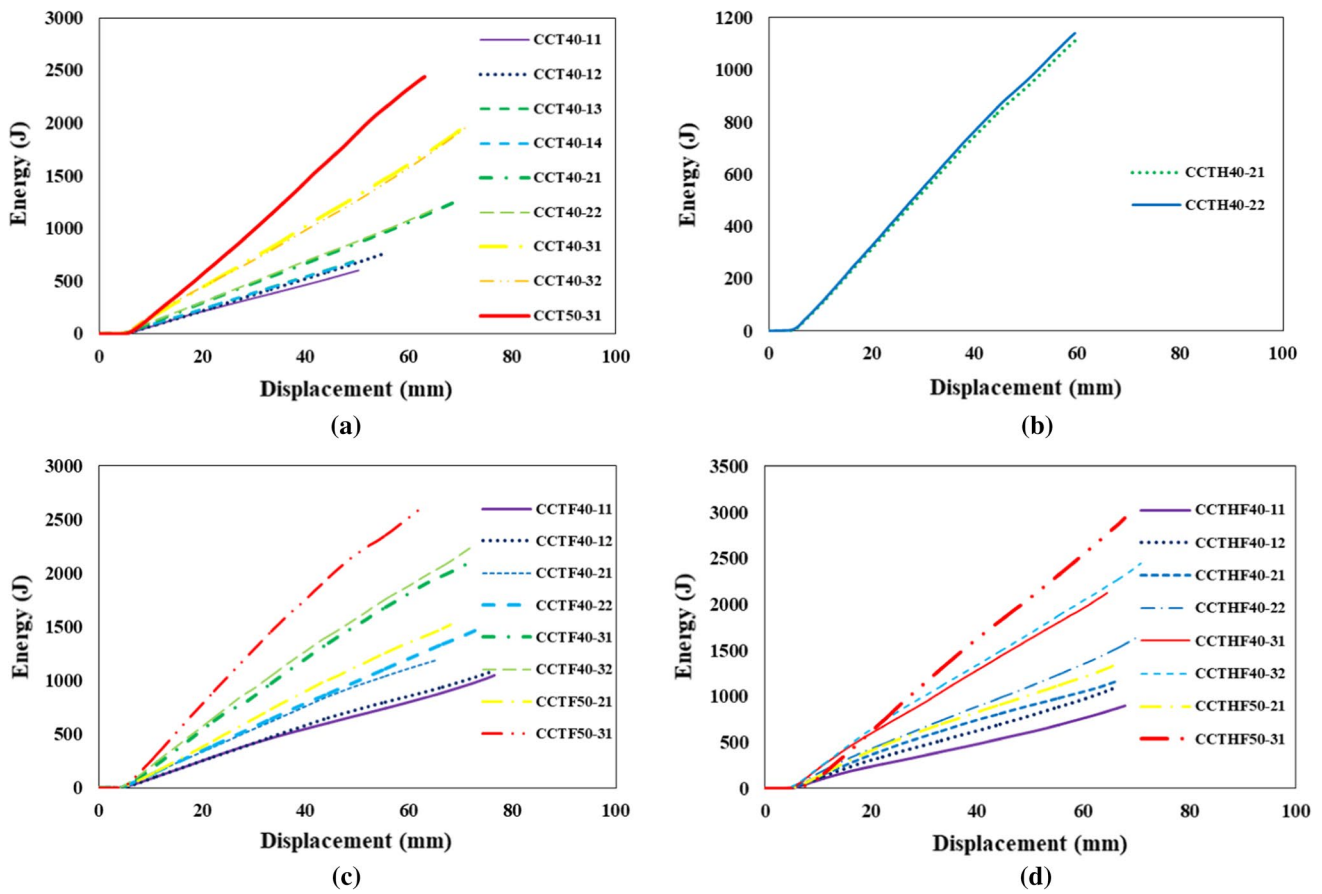


Fig. 15 Crash load–displacement diagrams for: a hollow tubes; b honeycomb-filled tubes; c foam-filled tubes; d foam/honeycomb-filled tubes



**Fig. 16** Energy-displacement diagrams for: **a** hollow tubes; **b** honeycomb-filled tubes; **c** foam-filled tubes; **d** foam/honeycomb-filled tubes

**Table 3** Crashworthiness characteristics of experimental results

Group no.	Sample	Length (mm)	Mass (g)	PCF (KN)	MCF (KN)	CFE (%)	EA (J)	SEA (J/g)
	H40-1	80	3.38	1.72	1.51	0.8779	91	26.92
	H40-2	40	1.69	1.70	1.45	0.8529	49	28.99
	HF40-1	80	8.6	3	3.17	1.0566	209.66	24.37
	F40-1	80	5.4	0.53	0.58	1.0943	38.45	7.12
1	CCT40-11	80	14.33	16.99	12.42	0.73142	820.17	57.234
1	CCT40-15	80	14.96	19.60	9.61	0.49030	634	42.37
1	CCT40-21	80	20.27	20.9	18.04	0.86342	1191	59.90
1	CCT40-31	80	29.84	33	27.63	0.8292	1806	60.52
1	CCT50-31	80	38.66	43	38.72	0.9016	2559	66.19
2	CCTH40-21	80	23.96	22.77	18.66	0.8194	1232	51.41
3	CCTF40-12	80	18.20	18.06	14.12	0.7819	932	51.20
3	CCTF40-22	80	23.69	20.38	20.15	0.9887	1330	56.14
3	CCTF40-32	80	35.98	40.7	31.13	0.7650	2055	57.11
3	CCTF50-31	80	46.88	53.29	41.81	0.7847	2760	58.87
4	CCTHF40-12	80	24.56	22.2	16.61	0.7483	1096	44.64
4	CCTHF40-22	80	29.62	31.5	22.92	0.7277	1513	51.08
4	CCTHF40-32	80	41.29	47.1	34.12	0.7244	2252	54.54
4	CCTHF50-31	80	52.74	52.84	43.07	0.8152	2843	53.90

compression of outer tubes shells is ensured and the value of EA is increased.

The combination of foam and honeycomb prevents the formation of internal frond and only the external frond is formed. In fact, the combination of honeycomb and foam in foam/honeycomb-filled tubes (CCTHF) causes deformation and collapse of Mode I-b. As shown in Fig. 17 the end-crushing mode (Mode I) of composite tubes can be divided into two categories, Mode I-a, and Mode I-b. Combining foam and honeycomb in foam/honeycomb-filled tubes (CCTHF) in addition to absorbing energy by foam and honeycomb, the interaction between honeycomb foam also absorbs a lot of energy which increases the EA and MCF. Based on experimental results and Eqs. (4) and (11), the EA and MCF in foam/honeycomb-filled tubes (CCTHF) have seven main energy sources such as the fronds bending energy, energy owing to hoop strain, energy resulting from crack propagation, the energy of friction, energy due to honeycomb cell walls, energy due to densification of foam, and energy due to the interaction between honeycomb cell-walls filling foam.

As mentioned above, all the composite tubes are not crushed as the end-crushing mode (Mode I). Gary and Farley [49] discovered that the progressively crushing of composite tubes is depends on the structure of the tubes and how the fibers and matrices are combined. They showed that column instability may result in the failure of thin-wall tubes, and thick-wall tubes' failure may be in a circumferential tension failure mode. On the other word, the progressive crushing mode in the tubes possessing extremely thin or thick walls is not probable. Considering this phenomenon with respect to the obtained results for crushing shape of cylindrical composite tubes filled with foam and honeycomb in Fig. 14, it may be inferred that the combination of foam and honeycomb fillers helps the progressive crushing of composite tubes and prevents the catastrophic failure of the composite during the crushing process. This is due to the pressure of the foam and honeycomb fillers on the composite tube wall, which causes the composite wall to split. During the catastrophic failure, the peak force is quite large which rapidly decreases; hence, the average force is not high.

During the triggering process, the failure is initiated, preventing the transfer of load to the entire structure by creating

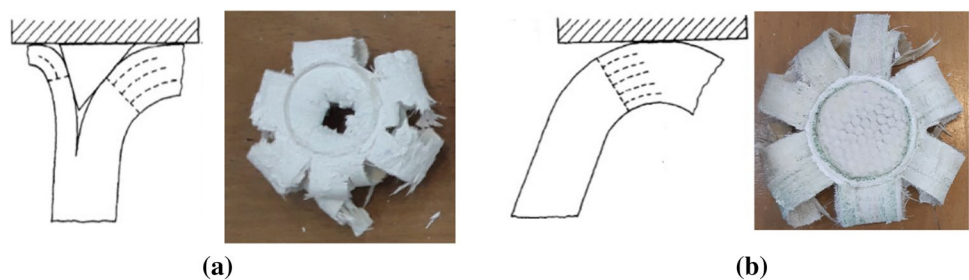
stress concentration on the edges of the profile geometry. Therefore, triggering hinder the catastrophically crushing of the composite structures. Considering the crushing shape of CCTHF tubes shown in Fig. 14, it is inferred that the combination of foam and honeycomb fillers acts as a trigger by creating pressure on the tube's wall.

According to Figs. 18 and 19 and Table 3, the PCF, MCF and EA of foam/honeycomb-filled tubes exceed than that of other tubes of other groups, whereas CFE remains almost constant. In addition, SEA of tubes filled with both foam and honeycomb is lower than that of other tubes of other groups because the solidity ratio of honeycomb and foam used in this study was low.

To clarify and better understand the catastrophic failure in composites tubes, performed a quasi-static load test on a sample of composite tubes (Group 1) with a thickness of 1.5 mm to investigate the collapse and deformation mode and obtain a crash load–displacement diagram. According to the crash load–displacement diagram shown in Fig. 11 and the shape of the sample during the crushing process shown in Fig. 20, it can be understood that the sample has suffered a catastrophic failure.

To better understand, a comparison study between crash load–displacement diagrams and the failure pattern of this sample with samples of composite tubes with a thickness of 1.5 mm by failure mode of end crushing mode (Mode I) has been performed. The crashworthiness characteristics of the samples are shown in Table 3. By comparing the crashworthiness characteristics of composite tubes (Group 1) with a thickness of 1.5 mm with different deformation mode, it can be seen that the tubes with end crushing mode (Mode I) is much higher crashworthiness characteristics than the tubes with catastrophic failure (Mode III). According to Table 3, EA and MCF of sample CCT40-11 with end crushing mode (Mode I) are 22.62% higher than the sample CCT40-15 with catastrophic failure (Mode III). Also, CFE and SEA of sample CCT40-11 with end crushing mode (Mode I) are 37.30% and 26% higher than the sample CCT40-15 with catastrophic failure (Mode III), respectively. Based on the experimental result, the use of the combination of foam and honeycomb fillers helps the end crushing mode (Mode I) of composite tubes. Therefore, one of the purposes of filling composite tubes with polyurethane foam and aluminum honeycomb is

**Fig. 17** Two categories of end-crushing mode (Mode I) of composite tubes: **a** Mode I-a, **b** Mode I-b





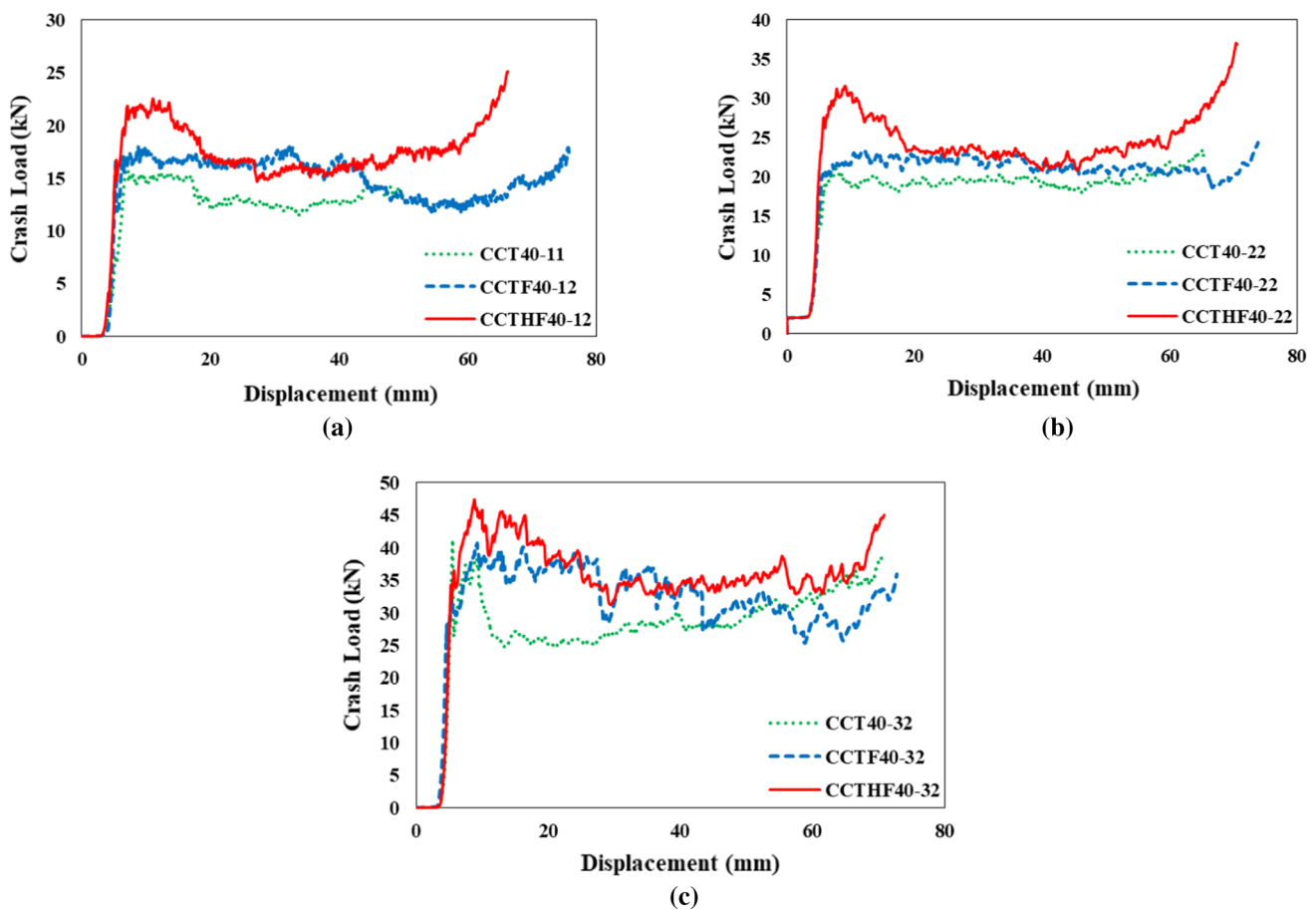


**Fig. 18** Comparison of crash load–displacement diagrams for hollow tubes, foam-filled tubes, and foam/honeycomb-filled tubes: **a** with wall thickness 1.5 mm; **b** with a 2-mm wall thickness; **c** with a 3-mm wall thickness

to prevent the catastrophic failure of the composite during the crushing process.

In other references [17, 38, 43] that used filler foam for composite tubes, only increased energy absorption and improved crushing shape are mentioned, and specific energy absorption has decreased. However, the results of some studies [17, 38] show that by increasing the foam density, the specific energy absorption of composite tubes will be increased.

#### 4.6 Effect of foam on honeycomb

In this investigation, polyurethane foam-filled aluminum honeycombs with an 80-mm height were investigated once subjected to quasi-static compression at the constant strain rate of 5 mm/min. These samples bear similarities with the core employed to fill hollow tubes (Group 4) in the current research. Two cylindrical honeycombs were filled with polyurethane foam to determine the crushing behavior of a combination of foam and honeycomb core with an 80-mm height. Figure 21 demonstrates the crash load–displacement

diagrams acquired from the quasi-static compression test conducted on one of the foam-filled honeycomb samples and its constituent components. It shows that the MCF of the foam-filled honeycomb significantly exceeds the summation of the MCF of its components. It is due to the interaction between honeycomb cell walls and the filling foam. The findings by Mahmoudabadi and Sadighi [7] revealed that the MCF of polyurethane foam-filled aluminum honeycomb exceeded the sum of MCF for foam and hollow honeycomb. An increase in the percentage of MCF results from the densities and solidity ratio of both polyurethane foam and honeycomb. According to Fig. 21 and Table 3, CFE of foam is much more than the honeycomb, which is improved the CFE of polyurethane foam-filled aluminum honeycombs.

#### 4.7 Effect of thickness of wall tubes

According to Fig. 22 and Table 3, when the wall thickness of hollow tubes and foam/honeycomb-filled tubes increase, PCF, MCF, EA, and SEA enhance, too. It is due to the higher volume of the material that cooperates in the plastic

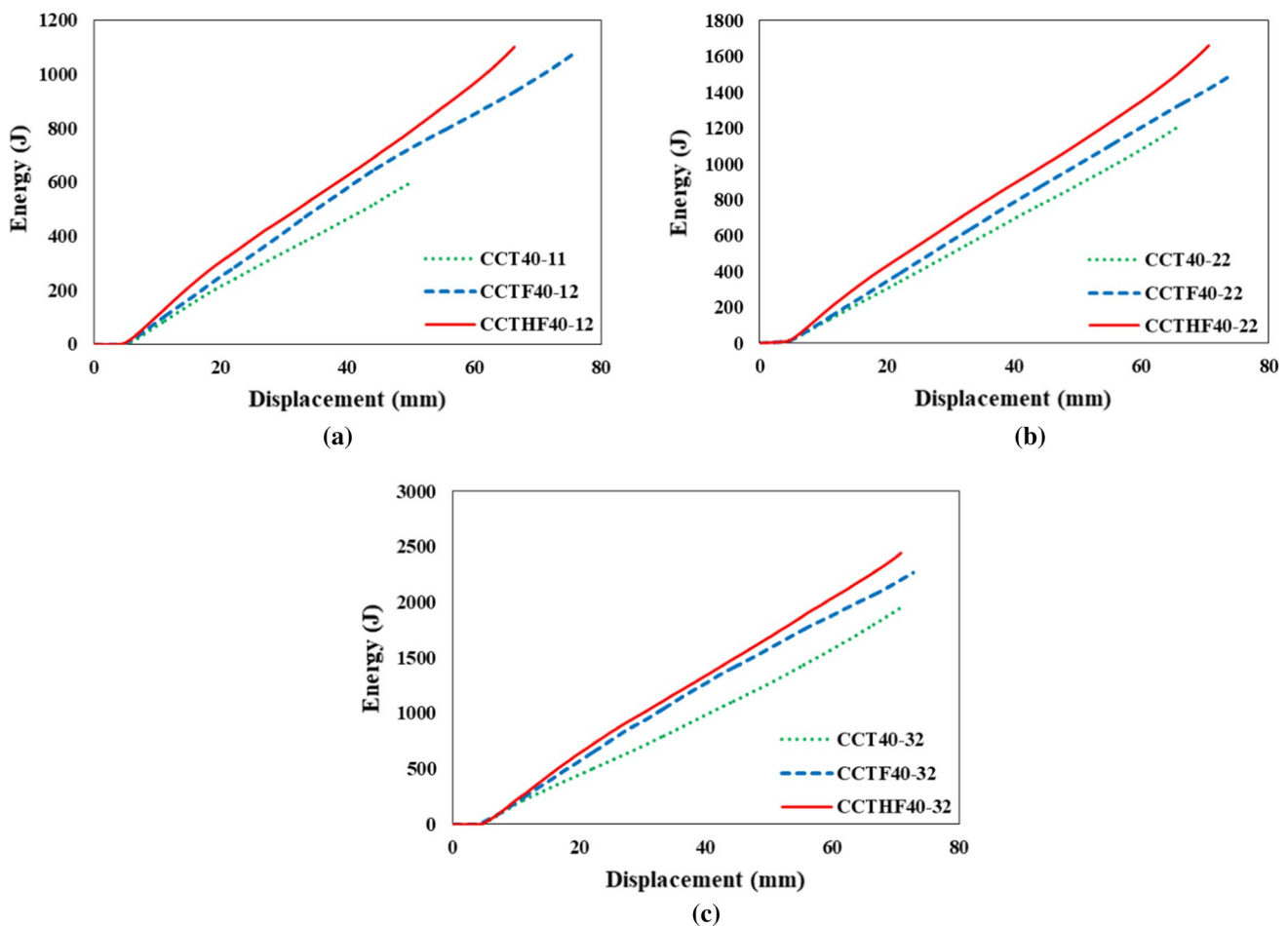


**Fig. 19** Comparison of energy-displacement diagrams for hollow tubes, foam-filled tubes, and foam/honeycomb-filled tubes: **a** with wall thickness 1.5 mm; **b** with a 2-mm wall thickness; **c** with a 3-mm wall thickness

deformation. However, CFE remains almost constant. As the wall thickness of the tubes increases, the impact of foam and honeycomb fillers on the EA, MCF decreases as shown in Table 4. Mean crushing forces of the hollow tubes CCT40-11 and CCT40-31 during the crushing process are equal to 12.42 and 27.63 KN, respectively, at the same displacement of 66 mm. Moreover, the EA of samples CCT40-11 and CCT40-31 are respectively equal to 820.17 and 1806 J, and therefore, the EA of sample CCT40-31 is 120.20%, which exceeds that of the samples CCT40-11. In other words, the EA of a tube with a wall thickness of 3 mm is 120%, which exceeds that of a tube with a 1.5-mm wall thickness.

Based on experimental results, it can be seen that increasing the wall thickness is directly related to the EA, MCF, and SEA of the composite tubes. According to Eq. (4), the EA and MCF of the composite tubes are a function of three variables of  $h$ ,  $t_1$  and  $\alpha$ , depending upon three geometric parameters of  $\emptyset$ ,  $R$  and  $T$ . As the wall thickness increases the thickness of the bended layers in the inwards and outwards directions of the shell radius is increases. Increases

the thickness of the bended layers in the inwards and outwards directions cause increases the bending energy. Also as the wall thickness increases, the friction at the interface between the wedge and the fronds and the friction at the interface between the platen and the petal are increases. In other words, the wall thickness of the composite tubes, such as bending energy, the hoop energy, the energy needed for circumferential delamination, and friction energy has a direct effect. The crushing behavior was dependent on the tube dimensions. Hamada and Ramakrishna [50] showed that tubes with  $t/D$  ratios smaller than 0.015 crashed by brittle fracture mode. This was attributed to the elastic instability of thin-walled tubes under axial compression load. Tubes with  $t/D$  ratios higher than 0.015 crushed progressively. Specific energy absorption capability was dependent on the absolute value of  $t$  rather than the  $t/D$  ratio. It increased with increasing  $t$  up to a certain value above which it decreased. Highest energy absorption capability was displayed by the tubes with values of  $t$  in the range 2–3 mm.

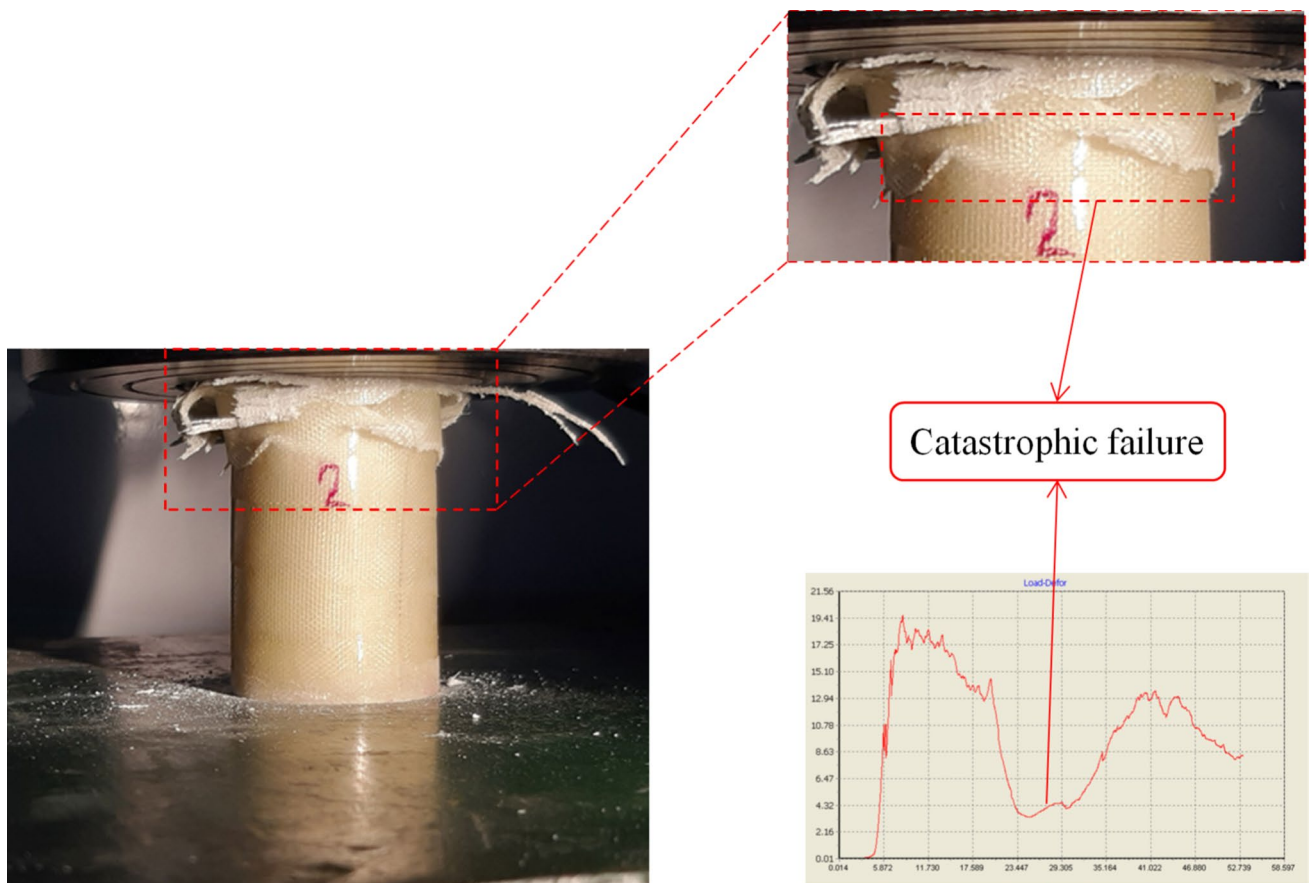


Fig. 20 Crash load–displacement diagram and the shape of the sample CCT40-15 during the crushing process

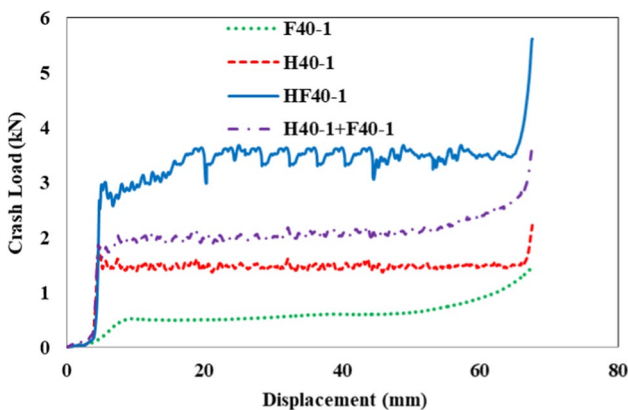


Fig. 21 Crash load–displacement diagrams of a honeycomb sample and its corresponding components subjected to quasi-static compression loading

#### 4.8 Effect of inner diameter of tubes

According to Fig. 23 and Table 3, when the inner diameter of the hollow tubes and foam/honeycomb-filled tubes increases, PCF, MCF, EA, and SEA enhances, too. It is due

to the higher volume of the material that cooperates in the plastic deformation. However, CFE remains almost constant. At the same displacement of 66 mm, mean crushing forces of the hollow tubes CCT40-31 and CCT50-31 during the crushing process are equal to 27.63 and 38.72 kN, respectively. Moreover, absorbed energy of the samples CCT40-31 and CCT50-31 are 1806 and 2559 J, respectively, and hence, the absorbed energy by the sample possessing a larger inner diameter is 41.69% higher than the corresponding value of the other one.

Based on experimental results, it can be seen that increasing the inner diameter is directly related to the EA, MCF, and SEA of the composite tubes. According to Eq. (4), the EA and MCF of the composite tubes are a function of three variables of  $h$ ,  $t_1$ , and  $\alpha$ , depending upon three geometric parameters of  $\varnothing$ ,  $R$  and  $T$ . According to Eq. (4), when the inner diameter is increased, the bending energy, friction energy, and the energy needed for circumferential delamination are increased. Still, when the inner diameter is increased, the hoop energy is constant. In other words, the inner diameter of the composite on three primary sources of energy absorption of the composite tubes, such as bending energy, the energy needed for circumferential delamination, and

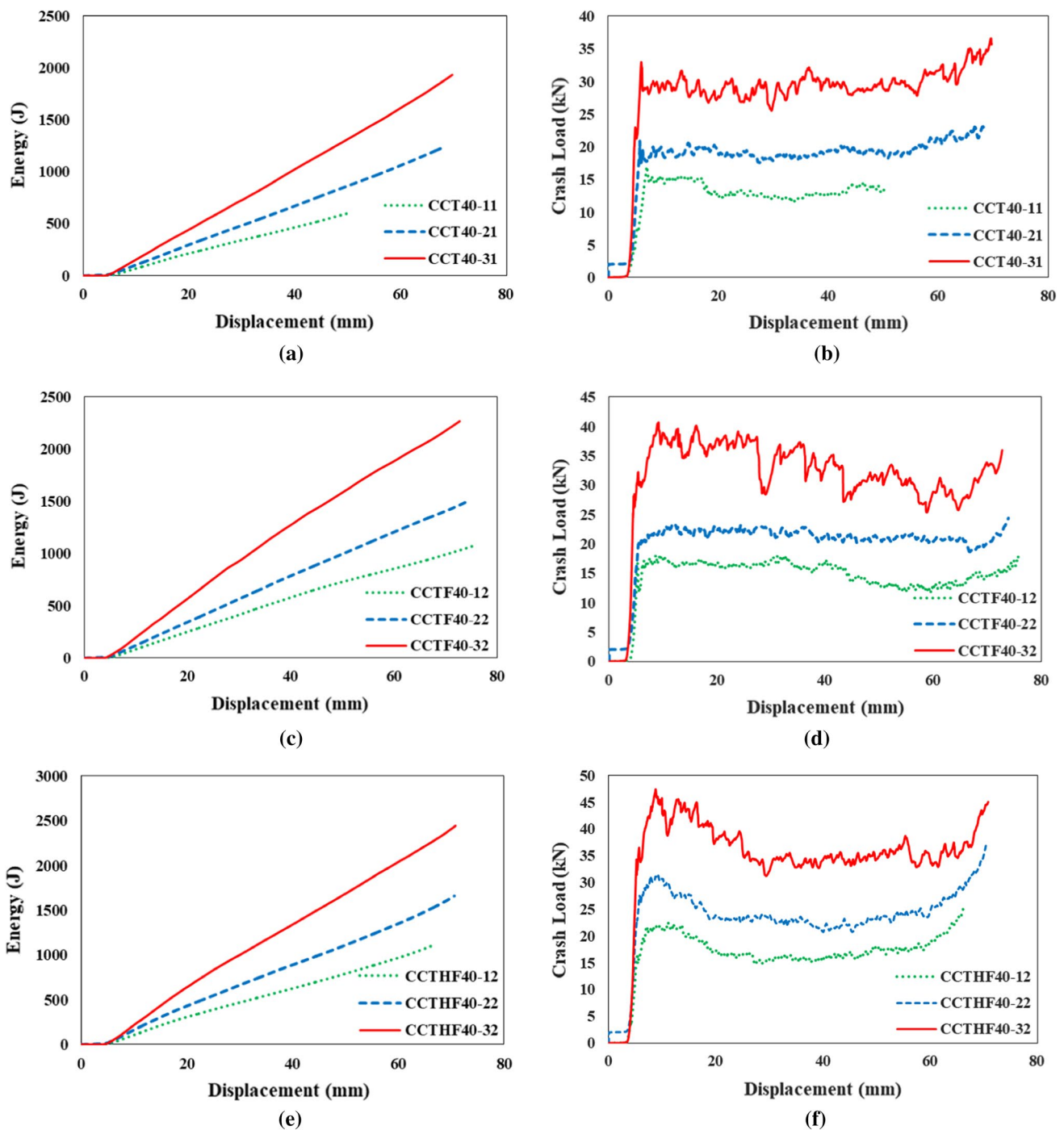


**Fig. 22** Comparison of energy-displacement and crash load-displacement diagrams for tubes with wall thickness 1.5, 2, and 3 mm: **a** energy-displacement diagrams for hollow tubes; **b** crash load-displacement diagrams for hollow tubes; **c** energy-displacement dia-

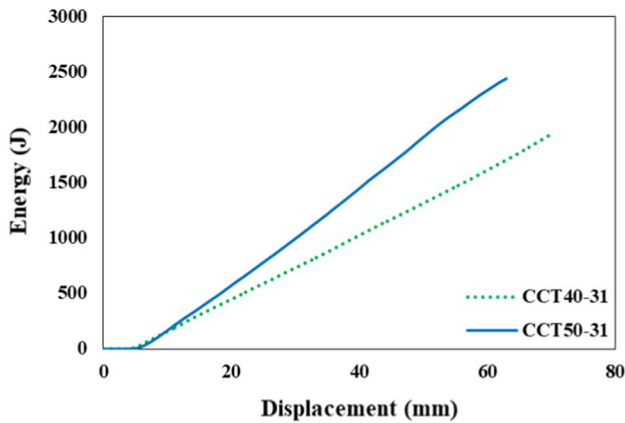
grams for foam-filled tubes; **d** crash load-displacement diagrams for foam-filled tubes; **e** energy-displacement diagrams for tubes filled with both foam and honeycomb; **f** crash load-displacement diagrams for foam/honeycomb-filled tubes

friction energy has a direct effect. As shown in Fig. 14, in foam/honeycomb-filled tubes, the number of external fronds increases from 6 to 7 by increasing the inner diameter of the tubes from 40 to 50 mm. Increasing the number of the frond, increases the energy required for propagation of the matrix

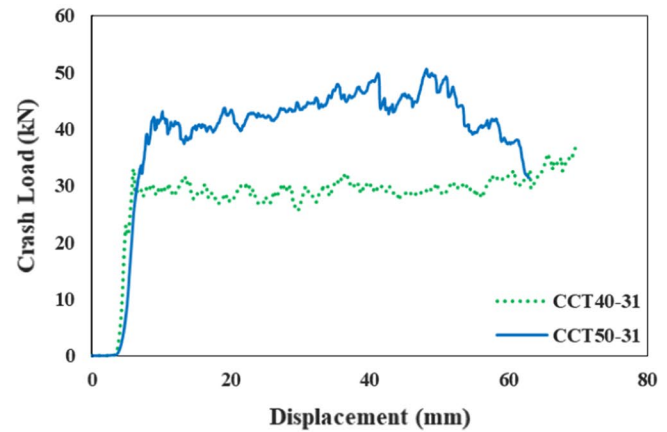
crack along the vertical direction (crack energy). According to the experimental results, increasing the wall thickness of the composite has a more impact on the crashworthiness characteristics of the composite tubes than increasing its inner diameter.

**Table 4** Comparison of EA and MCF of tubes of different wall thickness

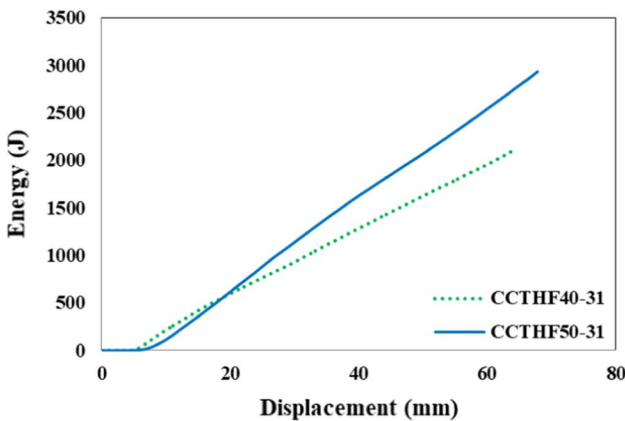
Group no.	Sample	Thickness (mm)	MCF (KN)	Increase (%)	EA (J)	Increase (%)
1	CCT40-11	1.5	12.42	–	820.17	–
3	CCTF40-12	1.5	14.12	13.63	932	13.63
4	CCTHF40-12	1.5	16.61	33.69	1096	33.69
1	CCT40-21	2	18.04	–	1191	–
2	CCTH40-21	2	18.66	3.43	1232	3.43
3	CCTF40-22	2	20.15	11.67	1330	11.67
4	CCTHF40-22	2	22.92	27.03	1513	27.03
1	CCT40-31	3	27.63	–	1806	–
3	CCTF40-32	3	31.13	13.78	2055	13.78
4	CCTHF40-32	3	34.12	24.69	2252	24.69



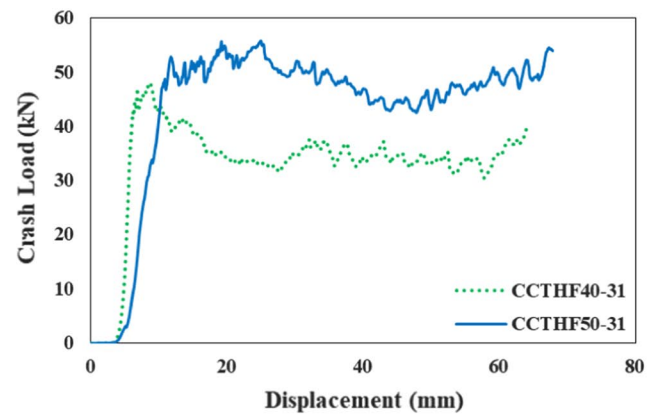
(a)



(b)



(c)



(d)

**Fig. 23** Comparison of energy–displacement and crash load–displacement diagrams for tubes with an inner diameter of 40 and 50 mm: **a** energy–displacement diagrams for hollow tubes; **b** crash load–dis-

placement diagrams for hollow tubes; **c** energy–displacement diagrams for foam/honeycomb-filled tubes; **d** crash load–displacement diagrams for foam/honeycomb-filled tubes

### 4.9 Effect of honeycomb core on tubes

Crash load–displacement and energy absorb–displacement diagrams for the tubes filled with honeycomb are displayed

in Figs. 15b and 16d respectively. As it is expected, the PCF, MCF, and total EA of honeycomb-filled tubes exceed that of hollow tubes, and the SEA and CFE of honeycomb-filled tubes are smaller than that of hollow tubes because

the solidity ratio of honeycomb used in this study was low and not adhesive was used between the wall of the composite tubes and the honeycomb. Figure 24 indicates the collapse and deformation mode of tubes filled with honeycomb (Group 2) with a 40-mm inner diameter and a 2-mm wall thickness in circumference crack in the mid-length (Mode III).

In the honeycomb-filled tubes crush zone, internal frond, external frond, circumferential crack, honeycomb compaction, delamination, interlaminar delamination, and fragmentation of tube wall were observed that shown in Fig. 24. It should be noted that each of these failures causes energy absorption.

#### 4.10 Comparison of analytical and experimental result

According to the deformation and collapse of all tubes investigated in this study, the present analytical model can be employed to determine the mean crushing force. The present approach considers the interaction between cell walls of honeycomb and the foam filler. To obtain the mean crushing force of the composite tubes for all groups, used Eq. (4) in which  $\theta = 0$  because the composite cylindrical shell is a specific state of the conical configuration which is obtainable assuming the cone angle  $\theta$  equal to 0.  $\sigma_0$  is the ultimate stress in uniaxial tension of the laminate obtained from Fig. 7c,  $G$  is the critical strain energy release rate per unit interlaminar delaminated crack area equal to 0.58 kJ/m<sup>2</sup> [51],  $\mu_1$  is the coefficient of friction between frond and platen equals 0.35 [28],  $\mu_2$  is the coefficient of friction between the wedge and the fronds equal to 0.35 [28],  $d_c$  is determined from Eq. (5), and the parameters  $R$  and  $T$  are determined from Table 2. The nonlinear Eq. (4) aims at finding the critical values of the length  $h$ , the thickness  $t_1$ , and the opening angle  $\alpha$  with

the minimum mean load. The analytical minimization of the nonlinear Eq. (4) is not easy since the mean force gradient is not easy to nullify, hence, a numerical approach for optimization is required. Due to the generalizing of the model presented in Sect. 2, for independent variables above three, the numerical algorithm L-BFGS-B, which stands for limited memory Broyden–Fletcher–Goldfarb Shanno method for bound constrained optimization [52], was used. It should be noted that the crush length  $h$  is always positive, and the thickness of the plies bending outward the shell radius  $t_1$  belongs to the interval  $[0, T]$ .

For determining the mean crushing force of the foam, honeycomb, and interaction between honeycomb cell walls and the filling foam for (Group 2), (Group 3), and (Group 4) used Eq. (11) in which  $\sigma_f^*$  is flow stress of the foam equals 0.42 MPa,  $\varepsilon_f^*$  is densification strain equals 0.65. The flow stress,  $\sigma_0$  of AL 5052-H39 is 267.6 MPa [6], and  $S$  is the cell size determined from Table 2. To assess the effectiveness of the idealized model, some cases from the tests were investigated. Table 5 lists the average crushing forces and the percentage errors between the explained method and the results of the experiments for the geometrical cases considered.

Based on the theoretical model proposed, the distribution of the released energy of crush foam/honeycomb-filled tubes (Group 4) to the seven main energy sources was estimated as energy because of fronds bending about 25%, energy owing to hoop strain about 4.5%, energy resulting from crack propagation about 1.5%, the energy of friction about 39%, energy due to honeycomb cell walls about 15%, energy due to densification of foam about 6%, and energy due to the honeycomb cell walls- filling foam interaction between about 9% of the total one. In this proposed theoretical model, the interaction between the wall of the tube with foam and honeycomb is not considered. In the future for more accurate predictions of the mean crushing force, the effect of the interaction of

**Fig. 24** Deformation mode of honeycomb-filled tubes (Group 2)

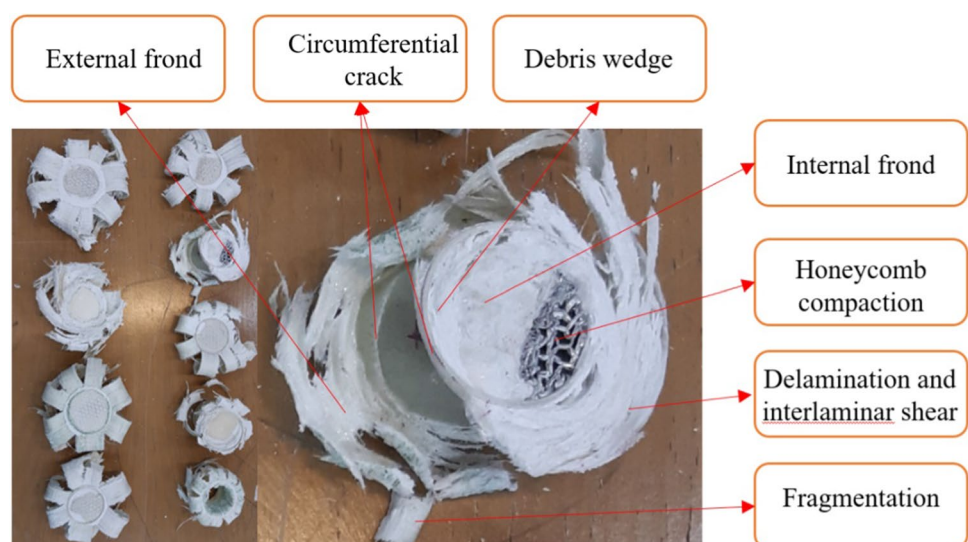


**Table 5** Comparison of mean crushing force of analytical and experiment

Group no.	Sample	Length (mm)	Mass (g)	MCF (experiment) (KN)	MCF (analytical) (KN)	Error (%)
	H40-1	80	3.38	1.51	1.35	10
	H40-2	40	1.69	1.45	1.33	8
	HF40-1	80	8.6	3.17	2.76	11
	F40-1	80	5.4	0.58	0.56	3
1	CCT40-11	80	14.33	12.42	13.28	7
1	CCT40-21	80	20.27	18.04	18.94	5
1	CCT40-31	80	29.84	27.63	28.45	3
1	CCT50-31	80	38.66	38.72	40.65	5
2	CCTH40-21	80	23.96	18.66	20.15	8
3	CCTF40-12	80	18.2	14.12	15.24	8
3	CCTF40-22	80	23.69	20.15	21.35	6
3	CCTF40-32	80	35.98	31.13	32.37	4
3	CCTF50-31	80	46.88	41.81	44.31	6
4	CCTHF40-12	80	24.56	16.61	18.32	10
4	CCTHF40-22	80	29.62	22.92	24.75	8
4	CCTHF40-32	80	41.29	34.12	36.16	6
4	CCTHF50-31	80	52.74	43.07	46.51	8

the wall of the tube with foam and honeycomb can be considered in the current theoretical model.

According to the analytical study of this article and the other research [17, 34, 38], it can be concluded that by increasing the foam density, the specific energy absorption of CCTHF tubes will be increased. To confirm this issue, the SEA of the foam/honeycomb-filled tube CCTHF50-31 with two foams with higher densities than the foam density used in this study, using the relations of the analytical study of this research, in Table 6 is presented. The SEA of these samples was compared with that of the corresponding hollow tube, the CCT50-31 tube. It should be noted that to obtain the SEA, the EA is divided by the weight of the crushing length of the samples, not the total weight of the tubes. The density, densification strain, and flow stress of Foam 2 are 90 kg/m<sup>3</sup>, 0.7, and 0.89 MPa [7] respectively. The density, densification strain, and flow stress of Foam 3 are 200 kg/m<sup>3</sup>, 0.55, and 7 MPa [34] respectively. The crushing lengths and EA of foam/honeycomb-filled tubes depend on the densification strain of foam and honeycomb. Because the honeycomb characteristics have not changed,

the crushing length has been considered to calculate the specific energy absorption based on high-density foam densification strain (Foam 3). Therefore, to ensure that none of the foam/honeycomb-filled tubes of different densities reach the densification strain. The crushing length is equal to 44 mm based on the densification strain of Foam 3. The results of Table 6 show that with increasing foam density, the MCF, EA, and SEA increase. Also, the results show that foam/honeycomb-filled tubes have a high potential for energy absorber compared to hollow tubes. It is important to note that as increasing the density of foam and honeycomb, the crush length is reduced. To optimize the crashworthiness characteristics of foam/honeycomb-filled tubes, it is necessary to study the effective parameters in the future.

## 5 Conclusions

Due to the lack of a comprehensive study on the crashworthiness characteristics of cylindrical composites filled with foam and honeycomb this study was performed to

**Table 6** Analytical study of crashworthiness characteristics of CCTH50-31 of different Foam densities

Group no.	Sample	Crush length (mm)	Mass (g)	Foam number	Foam density (kg/m <sup>3</sup> )	MCF (KN)	EA (J)	SEA (J/g)
1	CCT50-31	44	21.26	–	–	37.09	1632	76.76
4	CCTHF50-31	44	29	Foam 1	55	41.13	1810	62.31
4	CCTHF50-31	44	39.69	Foam 2	90	63.5	2794	70.40
4	CCTHF50-31	44	49.34	Foam 3	200	87.91	3868	78.40

a comparison study of the effect of these fillers and their combination together on the crashworthiness characteristics and deformation mode of cylindrical composite tubes. This study presented an analytical model for the crushing behavior of the cylindrical composite shell filled with foam and honeycomb materials under quasi-static load. The presented analytical model which is based on the energy method is applied to make predictions on the mean crushing force during the collapse process. In this study, according to the experimental observations, the stable mode of collapse (Mode I) which has the ability to absorb the most energy is considered for composite cylindrical shells. In this analytical method, the main contribution of the shell, honeycomb, and foam EA which are shell bending, petal formation, circumferential delamination, friction, the collapse of honeycomb cell walls, deformation of foam is considered to determine total internal energy during the crash process. This energy is equal to the work performed by the external load. Then axial crushing tests were run with cylindrical hollow composite tubes (Group 1), CCTH (Group 2), CCTF (Group 3), and CCTHF (Group 4). The test samples were 80 mm long and were exposed to quasi-static compression loads at the constant strain rate of 5 mm/s. The findings showed that the deformation mode of hollow tubes as well as CCTHF tubes was stable (Mode I). According to the obtained results, the collapse mode of CCTHF is much more stable compared to other groups' tubes. The most desirable samples in this study, in terms of MCF and EA, were CCTHF tubes, whose MCF increased up to 33% more than that of hollow tube samples. For CCTHF tubes, the highest increase in absorbed energy was 25%, compared with this parameter for hollow tubes. Considering the crushing shape of CCTHF tubes, it is inferred that the combination of foam and honeycomb fillers acts as a trigger by creating pressure on the tube's wall and prevents the catastrophic failure of the composite during the crushing process. As the wall thickness of the tubes increases, the impact of foam and honeycomb fillers on the EA, MCF, and CFE decreases. Finally, a comparison was made between the analytical and experimental results. By comparing the average crushing force obtained from the experimental and analytical results, it can be seen that the proposed analytical model has an acceptable predictive power for the behavior of CCTHF tubes.

## References

- Xiao X (2009) Modeling energy absorption with a damage mechanics based composite material model. *J Compos Mater* 43(5):427–444. <https://doi.org/10.1177/0021998308097686>
- Tomasz W (1983) Crushing analysis of metal honeycombs. *Int J Impact Eng* 1(2):157–174. [https://doi.org/10.1016/0734-743X\(83\)90004-0](https://doi.org/10.1016/0734-743X(83)90004-0)
- Weigang C, Tomasz W (2001) Relative merits of single-cell, multi-cell and foam-filled thin-walled structures in energy absorption. *Thin-Walled Struct* 39(4):287–306. [https://doi.org/10.1016/S0263-8231\(01\)00006-4](https://doi.org/10.1016/S0263-8231(01)00006-4)
- Li K, Gao X-L, Wang J (2007) Dynamic crushing behavior of honeycomb structures with irregular cell shapes and non-uniform cell wall thickness. *Int J Solids Struct* 44(14–15):5003–5026. <https://doi.org/10.1016/j.ijsolstr.2006.12.017>
- Mahmoudabadi MZ, Sadighi M (2009) A study on metal hexagonal honeycomb crushing under quasi-static loading. *World Acad Sci Eng Technol* 53:677–681
- Nia AA, Sadeghi M (2010) The effects of foam filling on compressive response of hexagonal cell aluminum honeycombs under axial loading-experimental study. *Mater Des* 31(3):1216–1230. <https://doi.org/10.1016/j.matdes.2009.09.030>
- Mahmoudabadi MZ, Sadighi M (2011) A study on the static and dynamic loading of the foam filled metal hexagonal honeycomb—theoretical and experimental. *Mater Sci Eng A* 530:333–343. <https://doi.org/10.1016/j.msea.2011.09.093>
- Sadighi M, Salami SJ (2012) An investigation on low-velocity impact response of elastomeric & crushable foams. *Central Eur J Eng* 2(4):627–637. <https://doi.org/10.2478/s13531-012-0026-0>
- Liu Q, Fu J, Wang J, Ma J, Chen H, Li Q et al (2017) Axial and lateral crushing responses of aluminum honeycombs filled with EPP foam. *Compos B Eng* 130:236–247. <https://doi.org/10.1016/j.compositesb.2017.07.041>
- Zhang Y, Liu Q, He Z, Zong Z, Fang J (2019) Dynamic impact response of aluminum honeycombs filled with expanded polypropylene foam. *Compos B Eng* 156:17–27. <https://doi.org/10.1016/j.compositesb.2018.08.043>
- Zarei H, Kröger M (2008) Optimum honeycomb filled crash absorber design. *J Mater Des* 29(1):193–204. <https://doi.org/10.1016/j.matdes.2006.10.013>
- Santosa S, Wierzbicki T (1998) Crash behavior of box columns filled with aluminum honeycomb or foam. *Comput Struct* 68(4):343–367. [https://doi.org/10.1016/S0045-7949\(98\)00067-4](https://doi.org/10.1016/S0045-7949(98)00067-4)
- Kılıçaslan C (2015) Numerical crushing analysis of aluminum foam-filled corrugated single-and double-circular tubes subjected to axial impact loading. *Thin-Walled Struct* 96:82–94. <https://doi.org/10.1016/j.tws.2015.08.009>
- Hussein RD, Ruan D, Lu G, Guillo S, Yoon JW (2017) Crushing response of square aluminium tubes filled with polyurethane foam and aluminium honeycomb. *Thin-Walled Struct* 110:140–154. <https://doi.org/10.1016/j.tws.2016.10.023>
- Yang F, Fan H, Meguid S (2019) Effect of foam-filling on collapse mode transition of thin-walled circular columns under axial compression: analytical, numerical and experimental studies. *Int J Mech Sci* 150:665–676. <https://doi.org/10.1016/j.ijmeccsci.2018.10.047>
- Zarei HR, Kröger M (2007) Crashworthiness optimization of empty and filled aluminum crash boxes. *Int J Crashworthiness* 12(3):255–264. <https://doi.org/10.1080/13588260701441159>
- Mahbod M, Asgari M (2018) Energy absorption analysis of a novel foam-filled corrugated composite tube under axial and oblique loadings. *Thin-walled Struct* 129:58–73. <https://doi.org/10.1016/j.tws.2018.03.023>
- Mamalis AG, Robinson M, Manolakos DE, Demosthenous GA, Ioannidis MB, Carruthers J (1997) Crashworthy capability of composite material structures. *Compos Struct* 37:109–134. [https://doi.org/10.1016/S0263-8223\(97\)80005-0](https://doi.org/10.1016/S0263-8223(97)80005-0)
- Jacob GC, Fellers JF, Simunovic S, Starbuck JM (2002) Energy absorption in polymer composite materials for automotive crashworthiness. *J Compos Mater* 36:813–850. <https://doi.org/10.1177/0021998302036007164>
- Mamalis A, Manolakos D, Demosthenous G, Ioannidis M (1997) Analytical modelling of the static and dynamic axial collapse



- of thin-walled fibreglass composite conical shells. *Int J Impact Eng* 19(5–6):477–492. [https://doi.org/10.1016/S0734-743X\(97\)00007-9](https://doi.org/10.1016/S0734-743X(97)00007-9)
21. Mahdi E, Mokhtar A, Asari N, Elfaki F, Abdullah E (2006) Non-linear finite element analysis of axially crushed cotton fibre composite corrugated tubes. *Compos Struct* 75(1–4):39–48. <https://doi.org/10.1016/j.compstruct.2006.04.057>
  22. Zarei H, Kröger M, Albertsen H (2008) An experimental and numerical crashworthiness investigation of thermoplastic composite crash boxes. *Compos Struct* 85(3):245–257. <https://doi.org/10.1016/j.compstruct.2007.10.028>
  23. McGregor C, Vaziri R, Xiao X (2010) Finite element modelling of the progressive crushing of braided composite tubes under axial impact. *Int J Impact Eng* 37(6):72–662. <https://doi.org/10.1016/j.ijimpeng.2009.09.005>
  24. Zhang Z, Liu S, Tang Z (2010) Crashworthiness investigation of kagome honeycomb sandwich cylindrical column under axial crushing loads. *Thin-Walled Struct* 48(1):9–18. <https://doi.org/10.1016/j.tws.2009.08.002>
  25. Niknejad A, Liaghat G, Naeini HM, Behraves A (2011) Theoretical and experimental studies of the instantaneous folding force of the polyurethane foam-filled square honeycombs. *Mater Des* 32(1):69–75. <https://doi.org/10.1016/j.matdes.2010.06.033>
  26. Feraboli P, Wade B, Deleo F, Rassaian M, Higgins M, Byar A (2011) LS-DYNA MAT54 modeling of the axial crushing of a composite tape sinusoidal specimen. *Compos A Appl Sci Manuf* 42(11):1809–1825. <https://doi.org/10.1016/j.compositesa.2011.08.004>
  27. Kathiresan M, Manisekar K, Manikandan V (2014) Crashworthiness analysis of glass fibre/epoxy laminated thin walled composite conical frusta under axial compression. *Compos Struct* 108:584–599. <https://doi.org/10.1016/j.compstruct.2013.09.060>
  28. Boria S, Pettinari S, Giannoni F (2013) Theoretical analysis on the collapse mechanisms of thin-walled composite tubes. *Compos Struct* 103:43–49. <https://doi.org/10.1016/j.compstruct.2013.03.020>
  29. Siromani D, Awerbuch J, Tan T-M (2014) Finite element modeling of the crushing behavior of thin-walled CFRP tubes under axial compression. *Compos B Eng* 64:50–58. <https://doi.org/10.1016/j.compositesb.2014.04.008>
  30. Boria S, Belingardi G, Giannoni F (2014) A crashworthy problem on composite structures using a mathematical approach. *Procedia Eng* 88:125–132. <https://doi.org/10.1016/j.proeng.2014.11.135>
  31. Hwang S-K, Hwang H-Y (2018) Theoretical approach for the mechanical behaviors of conical composite tubes considering fiber orientation errors under static loads. *Compos Struct* 183:84–95. <https://doi.org/10.1016/j.compstruct.2017.01.042>
  32. Sun G, Li S, Li G, Li Q (2018) On crashing behaviors of aluminium/CFRP tubes subjected to axial and oblique loading: an experimental study. *Compos B Eng* 145:47–56. <https://doi.org/10.1016/j.compositesb.2018.02.001>
  33. Sun GY, Li SF, Liu Q, Li GY, Li Q (2016) Experimental study on crashworthiness of empty/aluminum foam/honeycomb-filled CFRP tubes. *Compos Struct* 115:969–993. <https://doi.org/10.1016/j.compstruct.2016.06.019>
  34. Gan N, Feng Y, Yin H, Wen G, Wang D, Huang X (2016) Quasi-static axial crushing experiment study of foam-filled CFRP and aluminum alloy thin-walled structures. *Compos Struct* 157:303–319. <https://doi.org/10.1016/j.compstruct.2016.08.043>
  35. Elahi SA, Rouzegar J, Niknejad A, Assaei H (2017) Theoretical study of absorbed energy by empty and foam-filled composite tubes under lateral compression. *Thin-Walled Struct* 114:1–10. <https://doi.org/10.1016/j.tws.2017.01.029>
  36. Zhang Y, Zong Z, Liu Q, Ma J, Wu Y, Li Q (2017) Static and dynamic crushing responses of CFRP sandwich panels filled with different reinforced materials. *Mater Des* 117:396–408. <https://doi.org/10.1016/j.matdes.2017.01.010>
  37. Zhou J, Guan Z, Cantwell W (2018) The energy-absorbing behaviour of composite tube-reinforced foams. *Compos B Eng* 139:227–237. <https://doi.org/10.1016/j.compositesb.2017.11.066>
  38. Meriç D, Gedikli H (2022) Multi-objective optimization of energy absorbing behavior of foam-filled hybrid composite tubes. *Compos Struct* 279:114771. <https://doi.org/10.1016/j.compstruct.2021.114771>
  39. Yao R, Pang T, He S, Li Q, Zhang B, Sun G (2022) A bio-inspired foam-filled multi-cell structural configuration for energy absorption. *Compos B Eng* 238:109801. <https://doi.org/10.1016/j.compositesb.2022.109801>
  40. Wang H, Wang W, Wang P, Jin F, Fan H (2021) Foam-filled lightweight braided-textile reinforced and nested tubular structures for energy absorption applications. *Compos A Appl Sci Manuf* 149:106569. <https://doi.org/10.1016/j.compositesa.2021.106569>
  41. Yao S, Chen Z, Xu P, Li Z, Zhao Z (2021) Experimental and numerical study on the energy absorption of polyurethane foam-filled metal/composite hybrid structures. *Metals* 11(1):118. <https://doi.org/10.3390/met11010118>
  42. Lykakos SS, Kostazos PK, Venetsanos OV, Manolakos DE (2021) Crashworthiness performance of aluminium, GFRP and hybrid aluminium/GFRP circular tubes under quasi-static and dynamic axial loading conditions: a comparative experimental study. *Dynamics* 1(1):22–48. <https://doi.org/10.3390/dynamics1010004>
  43. Yang C, Chen Z, Yao S, Xu P, Li S, Alqahtani MS (2022) Parametric study on the crushing performance of a polyurethane foam-filled CFRP/Al composite sandwich structure. *Polym Test* 108:107515. <https://doi.org/10.1016/j.polymertesting.2022.107515>
  44. Velmurugan R, Gupta NK, Solaimurugan S, Elayaperumal A (2004) The effect of stitching on FRP cylindrical shells under axial compression. *Int J Impact Eng* 30:923–938. <https://doi.org/10.1016/j.ijimpeng.2004.04.007>
  45. ASTM D3039. Standard test method for tensile properties of polymer matrix composite materials
  46. D1622/D1622M (2014) AI, Standard test method for apparent density of rigid cellular plastics, US
  47. D1621 (2010) AI, standard test method for compressive properties of rigid cellular plastics, US
  48. Mamalis AG, Manolakos DE, Demosthenous GA, Ioannidis MB (1998) *Crashworthiness of composite thin-walled structural components*. CRC Press
  49. Farley GL (1992) Crushing characteristics of continuous fiber-reinforced composite tubes. *J Compos Mater* 26(1):37–50. <https://doi.org/10.1177/002199839202600103>
  50. Hamada H, Ramakrishna S (1995) Scaling effects in the energy absorption of carbon-fiber/peek composite tubes. *Compos Sci Technol* 55:211–221. [https://doi.org/10.1016/0266-3538\(95\)00081-X](https://doi.org/10.1016/0266-3538(95)00081-X)
  51. Solaimurugan S, Velmurugan R (2007) Progressive crushing of stitched glass/polyester composite cylindrical shells. *Compos Sci Technol* 67(3–4):422–437. <https://doi.org/10.1016/j.compscitech.2006.09.002>
  52. Morales JL, Nocedal J (2011) Remark on “algorithm 778: L-bfgs-b: fortran subroutines for large-scale bound constrained optimization.” *ACM Trans Math Softw* 38(1):7:1–7:4. <https://doi.org/10.1145/2049662.2049669>

**Publisher's Note** Springer Nature remains neutral with regard to jurisdictional claims in published maps and institutional affiliations.